Graduate School Form 30
(Updated 11/20/2014)

# PURDUE UNIVERSITY
## GRADUATE SCHOOL
## Thesis/Dissertation Acceptance

This is to certify that the thesis/dissertation prepared

By Kunal R Khadke

Entitled

Material Design Using Surrogate Optimization Algorithm

For the degree of Master of Science in Mechanical Engineering

Is approved by the final examining committee:

Dr. Andres Tovar

Dr. Likun Zhu

Dr. El-Mounayri

To the best of my knowledge and as understood by the student in the Thesis/Dissertation Agreement, Publication Delay, and Certification/Disclaimer (Graduate School Form 32), this thesis/dissertation adheres to the provisions of Purdue University's "Policy on Integrity in Research" and the use of
copyrighted material.

Approved by Major Professor(s): Dr Andres Tovar

Approved by: Dr. Sohel Anwar 11/12/2014

Head of the Department Graduate Program Date

# MATERIAL DESIGN USING SURROGATE OPTIMIZATION ALGORITHM

A Thesis

Submitted to the Faculty

of

Purdue University

by

Kunal R Khadke

In Partial Fulfillment of the

Requirements for the Degree

of

Master of Science in Mechanical Engineering

May 2015

Purdue University

Indianapolis, Indiana

# ACKNOWLEDGMENTS

I would like to gratefully acknowledge my advisor, Andrés Tovar, whose guidance and encouragement made this work possible. I consider it a privilege to have worked with you and I will always be grateful for the substantial part you have played in my education as an engineer. In addition, I would like to thank the members of my committee, Likun Zhu and Hazim El-Mounayri. Through your instruction, you have both provided me with an invaluable source of knowledge over the years.

I would like to take this opportunity to thank my fellow researchers: Satyajeet Sinde, Kai Liu, Anahita Emami, Weigang An, and Ashish Kanna. It has been a pleasure to work with you all. Thank you for listening to my ideas. This research is much stronger having been exposed to your experience and encouragement. This research effort has been supported by The Air Force Office of Scientific Research - AFOSR FA9550-09-1-0633.

TABLE OF CONTENTS

Page

# LIST OF TABLES

# LIST OF FIGURES

Figure Page

# ABSTRACT

Khadke, Kunal R. M.S.M.E., Purdue University, May 2015. Material Design Using Surrogate Optimization Algorithm. Major Professor: Andrés Tovar.

Nanocomposite ceramics have been widely studied in order to tailor desired properties at high temperatures. Methodologies for development of material design are still under effect [1]. While finite element modeling (FEM) provides significant insight on material behavior, few design researchers have addressed the design paradox that accompanies this rapid design space expansion. A surrogate optimization model management framework has been proposed to make this design process tractable. In the surrogate optimization material design tool, the analysis cost is reduced by performing simulations on the surrogate model instead of high fidelity finite element model [2]. The methodology is incorporated to find the optimal number of silicon carbide (SiC) particles, in a silicon-nitride $Si_3N_4$ composite with maximum fracture energy [2]. Along with a deterministic optimization algorithm, model uncertainties have also been considered with the use of robust design optimization (RDO) method ensuring a design of minimum sensitivity to changes in the parameters. These methodologies applied to nanocomposites design have a significant impact on cost and design cycle time reduced.

# 1. INTRODUCTION

The research applications involving predicting the correct morphology of a composite material has not been developed to a large extent. This methodology involves advanced numerical tools for simulating material behavior which can also permit design optimization procedure. Therefore a methodology is needed to incorporate simulations in recur rations for optimization and also reducing the cost of optimization.

## 1.1 Justification: Need for Better Materials

The ongoing development of technological platforms in every field requires development of materials that would perform well at extreme and rough conditions. Finding materials which would perform well at high temperatures is of prime importance these days.

The advent of the modern jet-type power plant for aviation has greatly accelerated the development of new high-temperature ceramic materials. These power plants are essentially high-temperature engines which convert heat energy into work. The greater the differential in temperature of the air between the beginning and end of the conversion, the greater the efficiency of the engine. Consequently, turbo-jets, gas turbines, ram-jets and rockets have created a demand for materials which will withstand elevated temperatures [3].

Ceramic composites are also used in fuel cells [4]. The bipolar plates in fuel cells are made of materials like coated metal, graphite, flexible graphite, C-C composite and carbon-polymer composites among others.

All the above applications place demand on ceramic materials that can exhibit excellent properties at elevated temperatures and high loads. The growth of nanoscale materials for high temperature applications also places a demand for developing sim-

ulation methods of predicting the most suitable microstructural morphologies using robust optimization techniques.

## 1.2 Literature Review

The composite material design work has conventionally focused on strength, cost or stiffness without considering global and local tailoring of the structures [2, 5]. Haftka [6] used a stacked composite laminate to find an efficient composite material design by tailoring the thickness and orientation of the laminates [1]. Aronsson [7] predicted the strength of composites based on fracture energy using the damage zone model (DZM) by developing a notch in the composite material design. The damage zone model was shown to accurately predict fracture load, load- deformation behavior and damage zone sizes in these types of laminates.

A two-phase material characterization method was proposed by mapping non-linear, nonphysical regression parameters in microstructure correlation functions to a physically based, simple regression model of key material characteristic parameters [8]. A new descriptor based material design model of particle-based heterogeneous microstructures based on 2D images and then latter mapping it into a 3D model has been developed [9]. This design model cannot be used for reconstruction or in multiple iterative designs.

A multi-objective design objective algorithm called the artificial bee colony (ABC) was used on laminated composites to optimize the strength and the cost of the material [10]. A similar optimization of stacked laminated composite materials was carried out using a model with straight fiber layers using multiple optimization techniques [11]. A Reliability based optimization was also carried out 3D laminated composite shell structures. Delamination failures using the explicit non-linear finite element code was tested by a technique called as the matrix reinforced mixed theory in which several elements were stacked in a single finite element [12]. But the

multi-phase properties, morphology and the topologies of the composites have not been taken into consideration in the same algorithm.

Therefore, a novel simulation design is needed to incorporate the elasto-plastic properties of the composite material in the design and at the same time the design simulation should be generated in an iterative manner quickly. A design model is needed that can control the size of all phases in the composite for the purpose of optimization.

## 1.3 A Material Design Methodology

Nanomaterials are of great research interest in the past few years. Since the microstructural morphologies of these composites affect their properties to a large extent, it is very important to establish a design methodology and predict its behavior through simulation techniques [13]. Therefore, a simulation based design is needed to exploit computational material science and physics in accelerating the discovery of new materials [14]. Many researches have used the traditional methods like the Voronoi network [15] or the Lattice based model [16] for generating their designs. But very few have used it in iterations for solving problems of this type.

Morphology of a composite material the form in which different phases are arranged to form the structure of the material. The aim of this research is to predict the most suitable phase morphology of $Si_3N_4$ nanocomposites at room temperature and high temperature of 1400°C.The research serves as a good foundation for extending this methodology for other multiphase composites as well.

The difference between this work and the previous work presented is the characteristic of the model is the microstructure reconstruction with the change in input parameters. A novel contribution through this research is the generation of unique algorithm of creating a fixed mesh through the microstructure design. The design process is based on randomness. Therefore a random design, the finest finite element

mesh and a robust optimization algorithm provide a significant contribution to the material design optimization process.

A surrogate model algorithm is incorporated to the microstructural simulation and analysis code which further reduces the high fidelity function calls of the optimization process significantly [17, 18].

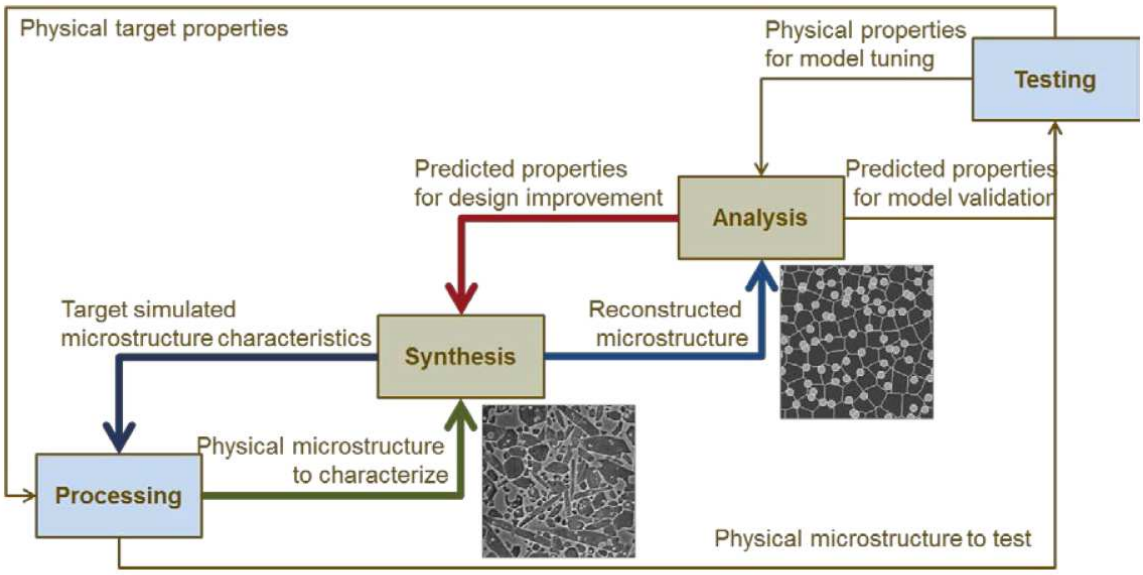


Figure 1.1. Composite Structure Design and Optimization Methodology

## 1.4 Research Objectives

A robust design model methodology incorporating the elasto-plastic properties along with user controllable characteristics of different phases in the composite which can be used in an iterative manner was not used in a surrogate optimization algorithm. Along with meticulously choosing the size of the simulation model, a consolidated approach of using the surrogate optimization technique in the current research is demonstrated with verification. The results obtained through this technique also

comply with the actual physical tests and material properties of the composite. No methodology of converting an image by pixel to element strategy has been developed for composite material design optimization.

The application of this design simulation technique in material optimization is demonstrated by using the fracture energy as the design variable. The optimization tool is applied to obtain an optimal number and size of the second phase Silicon Carbide particles along the Silicon Nitride grain boundaries with optimal fracture energy. The 2D design is based on randomness and reconstruction. The finite element model is based on a fixed mesh obtained from the 2D design. The uncertainty in the design is quantified which gives a robust design algorithm for finding the optimum morphology of a composite material. This design methodology can also be extended to any three or two phase composite material.

The first objective of this research is to create a microstructure reconstruction model with variable input design parameters. The optimization problem for determination of second phase size and number in the microstructure will be solved based on this model. The second objective will be to replicate this reconstruction model based on its properties in finite element software for determining its fracture energy. This approach will help in developing a statistically equivalent model for reconstruction every time it is generated. The third objective will be to quantify the uncertainties in the reconstruction model. As the reconstruction model will be based on randomness it will be important to quantify the uncertainties in the model to incorporate it in the robust surrogate optimization framework. The fourth objective will be to apply surrogate model optimization framework to the described methodology for reducing the expensive high fidelity function calls. As the explicit finite element problem will be time dependent, the high fidelity function calls will increase the time consumed for converging the optimization problem. The final objective will be to determine the optimal size and number of the second phase particles in the composite structure through this methodology.

## 1.5 Contribution in the Research

The 2D simulation model in Matlab is converted to a Finite Element Model by creating an interface between Matlab and LS-Dyna.LS-Dyna is chosen an explicit FEA solver for this research. A surrogate model based on radial basis function is generated in Matlab itself and linked with the high fidelity finite element model. The surrogate model generated in Matlab is also tested on a trial banana function which helps in building confidence in going ahead in going ahead and implementing that methodology in the material model design. The uncertainties in the model are also quantified using the Monte Carlo method. One iteration of the high fidelity model takes more than one hour and hence it takes easily more than one day to converge to a solution. The incorporation of surrogate model brings down the optimization convergence time to less than four hours because it uses very less of high fidelity function calls. The design methodology finds the optimum morphology at both the room temperature and the high temperature of 1400°C.

# 2. MICROSTRUCTURAL MODEL OF COMPOSITE CERAMICS

## 2.1 Microstructural Reconstruction

Creating microstructural simulations has become an integral part in material science and has been widely been accepted in research related to these topics. These simulations reduce the cost and time of performing actual physical simulations for different material samples required to perform the set of analysis. Assigning proper physical properties to the simulation and understanding relation between the physical structure and the simulation structure becomes an important part for successful computation of the experiment. Microstructure characterization is based on the features like the grain boundaries, grain size, grain orientation etc. Microstructures are characterized by grain sizes, phase dispersions, grain orientation in structure-property based simulations. The material properties can be controlled by tailoring the characteristics of the microstructure. In the material design the optimization algorithms are incorporated in the microstructure generation algorithm itself. In this way the microstructure is tailored comprehensively according to the need of the optimization algorithm. The Johnson-Mehl model and the Voronoi network models are the most well-known techniques for realistic microstructural representation.

In most of the microstructure generation algorithms randomly generated points serve as the nucleation sites for generation a grain structure.

### 2.1.1 Voronoi Network

The process which covers a plane with congruent plane figures is defined as a tessellation. Random numbers of points are generated in a plane [19]. Voronoi cells are constructed from these points by forming convex polygons. These cells grow in recurrence as long as all the generated points are covered in a particular plane.

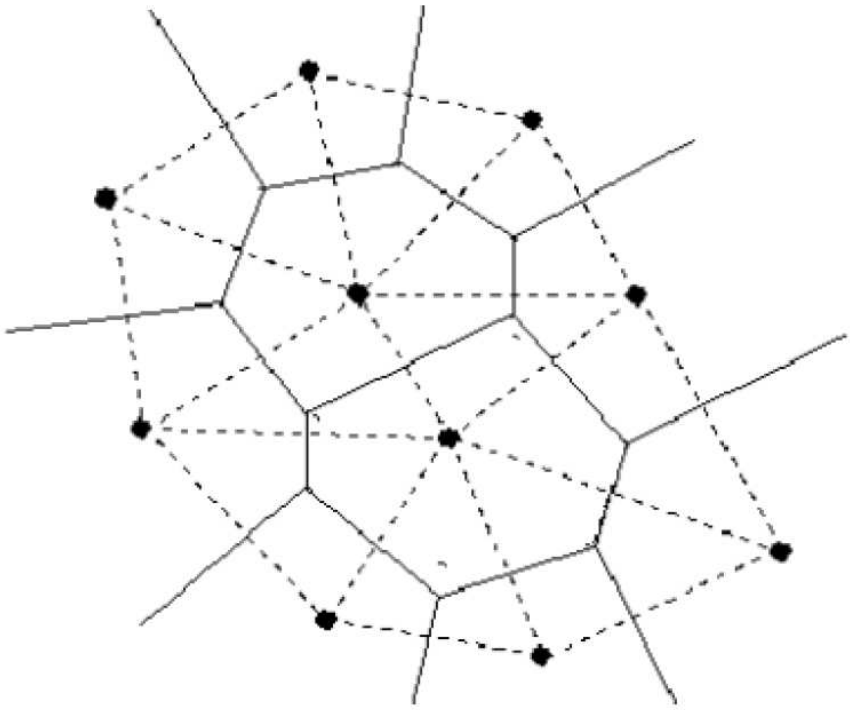

Figure 2.1. Vornoi network diagram [19]

When a line joining the points is shared by a side of a polygon Voronoi cells are created. The map generated by joining the points is called a Delaunay triangularization [20].

### 2.1.2 Johnson Mehl Model

The Johnson-Mehl model was first generated by Frost and Thompson [16].The Johnson Mehl model is based on the concept of grain growth. The nucleation sites are the randomly generated points same as in the Voronoi network. The grains begin to grow around the nucleation sites. The growth is time dependent which simulates a Poisson distribution by incrementing time of random intervals. The nucleation continues at one grain per unit time per unit of initial area till the entire plane is

covered. The total number of grains generated in a plane is thus dependent on the growth rate of nucleation.

After the growth rate is complete the triple points or the hyperbolic boundary between the grains determines the grain boundary. Figure 2.2 shows an example of John Mehl model.

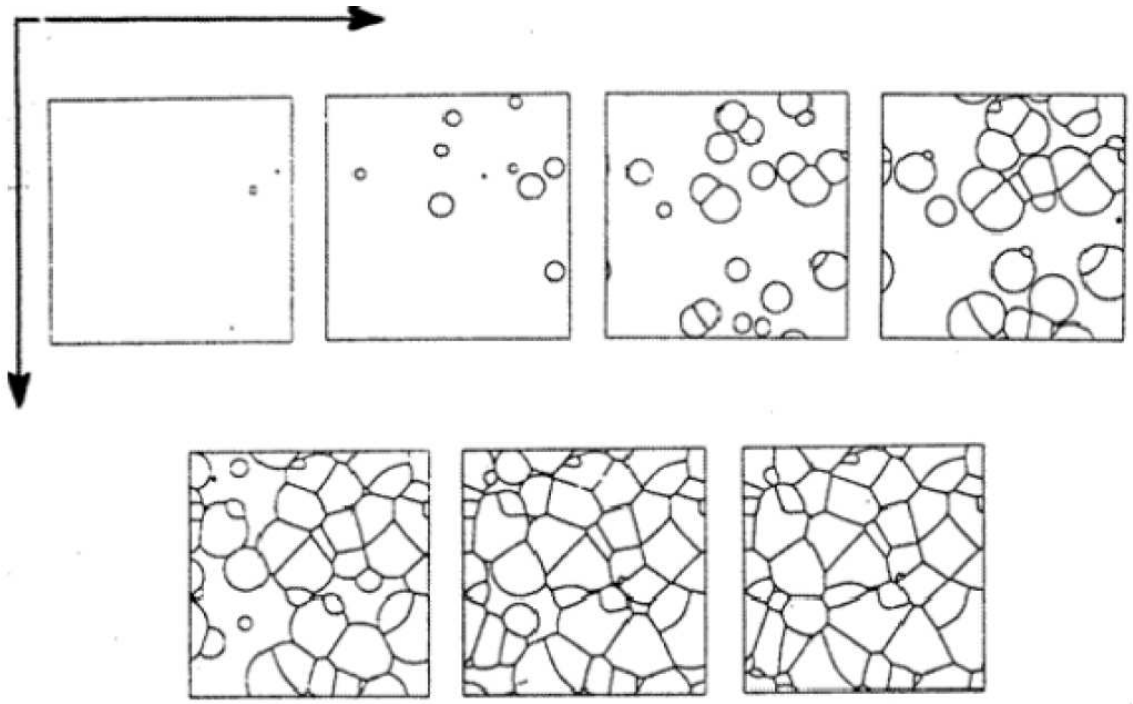

Figure 2.2. An example of the Johnson-Mehl model [21]

### 2.1.3 Cellular Automation Model (CA model)

The CA method uses physically based rules and provides a simpler physical realization of folding on a regular lattice in 2D and 3D. This model is computationally efficient and can be easily incorporated in a fixed-mesh finite element analysis framework. This work makes use of the CA method, which is extended to incorporate two-phase composite materials and crystalline orientation.

The microstructural simulation model incorporated in this work has two stages for each phase: nucleation and growth. Nucleation sites are randomly assigned preserving a critical box distance. The maximum number of nucleation sites is unknown a priori and should be determined by simulation.

The growth is defined by recrystallization kinetics of the parent phase surrounding the nucleation sites. The CA method incorporated determines the transformation of the parent phase in the neighborhood of a grain without regard of the energy field intruded by the grain, i.e., a neighboring parent phase is transformed with a given probability. The grain growth is therefore a function of both the neighborhood size and probability of transformation [22].

The neighborhood $N_i$ of a cell $i$ in a CA lattice is defined by

$$N_i = j : d(i, j) \leq r \tag{2.1}$$

where $d(i, j)$ is the distance between cells $i$ and $j$, and $r$ is the size of the neighborhood. If all neighboring parent-phase cells are transformed, the topology of the grain is determined by the size of the neighborhood as shown in Figure 2.3.

If the transformation occurs with a given probability $p$, such probability also determines the topology of the grain as shown in Figure 2.3. Bias can be incorporated by modifying the neighborhood layout. A comparison of models with and without bias is shown in Figure 2.4.

The user has good amount of control on the grain size, grain boundary size and the number of grains in the cellular automation model.

The grain boundary is identified using a CA rule and its thickness can be controlled with neighborhood size (Figure 2.6). The amorphous grain boundary has lower mechanical properties than the ceramic phases but, in moderate quantity, it increases the fracture energy of the CMC. The following sections deal with the numerical finite element model and the optimization method to determine the optimum microstructural layout.

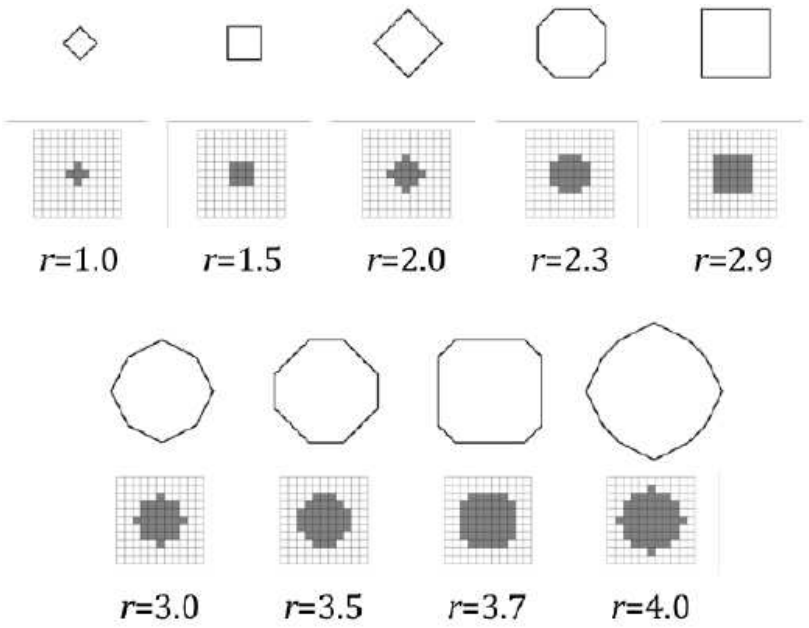


Figure 2.3. Grain topology as function of the CA neighborhood after a constant number of time steps. In each time step, all neighboring parent-phase cells are transformed.

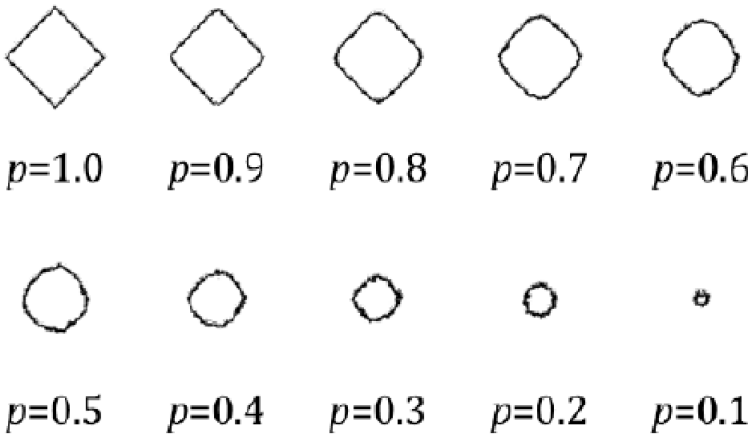


Figure 2.4. Grain topology as function of the probability $p$ of transformation after a constant number of time step for a neighborhood size $r = 1.0$.

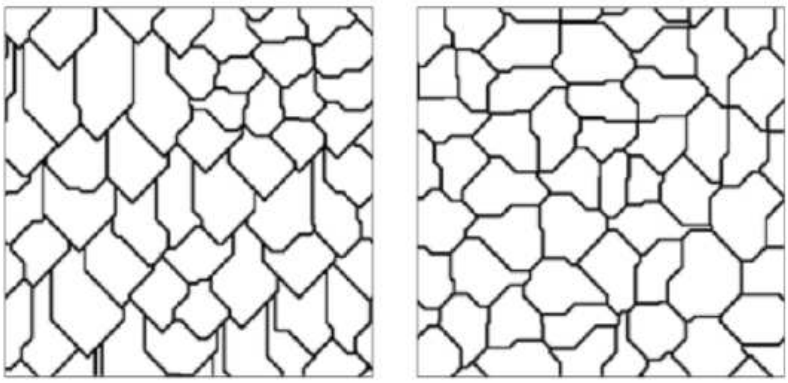

Figure 2.5. Microstructural for 40 grains, $r = 1.0$ and $p = 1.0$ with bias (left) and without bias (right).

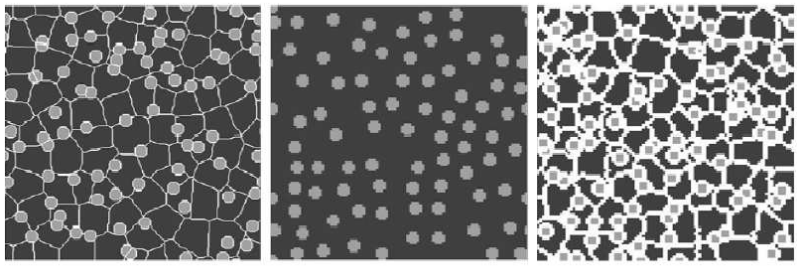

Figure 2.6. Microstructure with grain boundary size and resolutions: $1000 * 1000$ cells (Right) and $100 * 100$ cells (center and right).

# 3. FINITE ELEMENT MODEL FOR FRACTURE ANALYSIS

In this chapter a robust optimization tool using Surrogate Model Optimization methodology is incorporated to attain the optimal size and number of second phase Silicon Carbide (SiC) particles along the Silicon Nitride ($Si_3N_4$) grain boundaries to obtain a SiC- $Si_3N_4$ nanocomposite ceramic structure with maximum high and room temperature fracture energy. To study the properties of these nanocomposites it is important to find the behavior of these materials at both the room temperature as well as at temperatures of nearly 1400°C.

The main driving force for the interest of $Si_3N_4$-SiC composite materials has been their promise for high temperature applications. The $Si_3N_4$-SiC composite materials have distinctive behavior above 1200°Cin their fracture properties [23]. The primary initiation or the source of fracture are the grain boundaries.

## 3.1 Ceramic Matrix Composite Materials

The use of Ceramic Matrix Composites (CMCs) such as carbon fiber reinforced silicon carbide composites (C/SiC), carbon fiber reinforced carbon composites (C/C) but also silicon carbide fiber reinforced silicon carbide composites (SiC/SiC) is mandatory within the aerospace sector whenever the transfer of mechanical loads at high temperatures (up to 1900 K in air) is required and any metallic material (e.g. refractory metals) or intermetallic materials cannot be employed [24]. Ceramic matrix composite (CMC) materials can benefit aerospace in propulsion and exhaust, thermal protection, and hot primary structure applications.

The extremely good high temperature fracture toughness of CMCs is provided by the crack bridging effect of the carbon fibers: stress concentrations, e.g. notches or holes, are reduced by stress redistribution and inelastic deformation [25]. In case of

overloading, monolithic ceramics break immediately, while CMC materials are still able to carry load even if the elastic mechanical load range is exceeded. Such a damage tolerant behavior constitutes an important point for the safety issues in particular for space re-entry vehicles.

The Garrett engine (AGT 101) was an extension of the Ford 820 ceramic engine design [26]. It had a single shaft, a radial rotor, and air bearings. Many ceramic components fractured during testing, some due to design and assembly problems but most from material limitations. The desire was to use net-shape fabrication processes, but the state of technology in 1985 did not result in reliable ceramic turbine components. A CMC was therefore needed which has high fracture toughness at high temperatures. Hence, the Silicon Carbide-Silicon Nitride nanocomposite was found to be the solution for these applications and it is the prime area of focus in this investigation.

### 3.2 Observed Material Behavior

The properties and failure characteristics of ceramic materials change when the temperature increases. At room temperature the ceramics materials have no plastic strain and behave as brittle materials. But they gradually start weakening at around 900°C [27]. The failure mechanism is based on the phenomena of slow crack growth. The failure mechanism primarily is a function of the size of the grains, size and distribution of the grain boundary phase, the size of the distributed third phase particles. Through an experiment using a negative rake angled diamond cutting tool it was found that fracture is mainly a surface phenomenon and gradually presides through the cross-section of the solid. Hence, a 2D model with imbibed physical properties of the material can be used effectively to study the fracture initiation and to some extent growth as well [28].

### 3.2.1 Plastic Strain

The high temperature mechanical properties such as fracture energy or creep resistance of fine grained ceramics are controlled by their microstructure which determines the micro mechanisms of plastic deformation. Several ceramics have been found to exhibit enhanced ductility or even structural super plasticity at high temperature. Although these ceramics are very different with regard to microstructure, physical and chemical properties, they share one common feature that all of them have a very fine grain size (of the order of a micron or less).Consequently, grain boundaries (GBs) play a dominant role in the high temperature deformation process of these materials. Effectively, a major component of high temperature deformation is attributed to diffusion-accommodated GB-sliding [29].

A summary of experimental developments in nanoindentation of silicon by Domnich [30] revealed the elastic-plastic response and hysteresis of these normally brittle materials. The experiments showed that Si transforms from the cubic diamond phase to a metallic phase at elevated pressures. It was also found that it takes less energy to generate and propagate a crack (in a brittle material) than it takes to plastically deform the material.

The elastic behavior is specified by providing the elastic modulus and Poissons ratio. The strain hardening behavior is specified by a power law model given by

$$g(\varepsilon^p) = \sigma_0 \theta(T)[1 + \frac{\varepsilon^p}{\varepsilon_0^p}] \tag{3.1}$$

where, $g(\varepsilon^p)$ is the flow stress, $\sigma_0$ is the initial yield stress determined using the Drucker-Prager yield condition, $\theta(T)$ is the thermal softening factor, $n$ is the strain (work) hardening exponent and $\varepsilon^p$ and $\varepsilon_0^p$ are the accumulated plastic strain and reference plastic strain respectively [31].The Finite Element software LS-Dyna takes the value of effective plastic strain for considering the breakage criteria. The value of this effective plastic strain is always a fraction less than the real plastic strain value.

The simulations carried out in this research use a constitutive model that treats the material as elasto-plastic. Both the primary materials in the composite (i.e SiC and $Si_3N_4$ ) have very negligible plastic strain at the room temperatures. But at temperatures around 1400°C,silicon carbide shows a significant amount of plastic deformation before fracture [32]. In silicon nitride, the dislocations along the grain boundaries play a significant role for their plastic deformation along the grain boundaries. As the composition of the material plays an important part in observing the values of the plastic strain, it will always have a range of values for a specific temperature. The plastic strain of silicon carbide is taken as 0.05 and that of silicon nitride to be 0.02 at 1400°Cin the finite element simulations for this research [33].

### 3.2.2 Temperature Effect

Sintered $\alpha$-SiC shows an exceptional behavior of increasing flexural strength with increasing temperature when the tests are conducted in an open environment. But the 3 point bending strength results for $\alpha$-SiC shows a slight decrease in the elastic modulus with the increase in temperature [34].

## 3.3 Observed Fracture

$Si_3N_4$ shows plastic deformation characteristics at higher temperatures. The intergranular grain boundaries are found to be the primary mechanisms of fracture.

The grain boundaries are responsible for crack deection and accordingly damage is limited to a smaller geometric region in microstructures with grain boundaries. Hence, grain boundaries are the most influential phase in the microstructure for fracture propagation. On an average, a microstructure with grain boundaries present is stronger than the corresponding microstructure with grain boundaries removed because they tend to divert the line of fracture propagation.

The silicon carbide particles have higher elastic modulus than silicon nitride grains. In cases where the second phase SiC particles are in the wake of micro cracks the

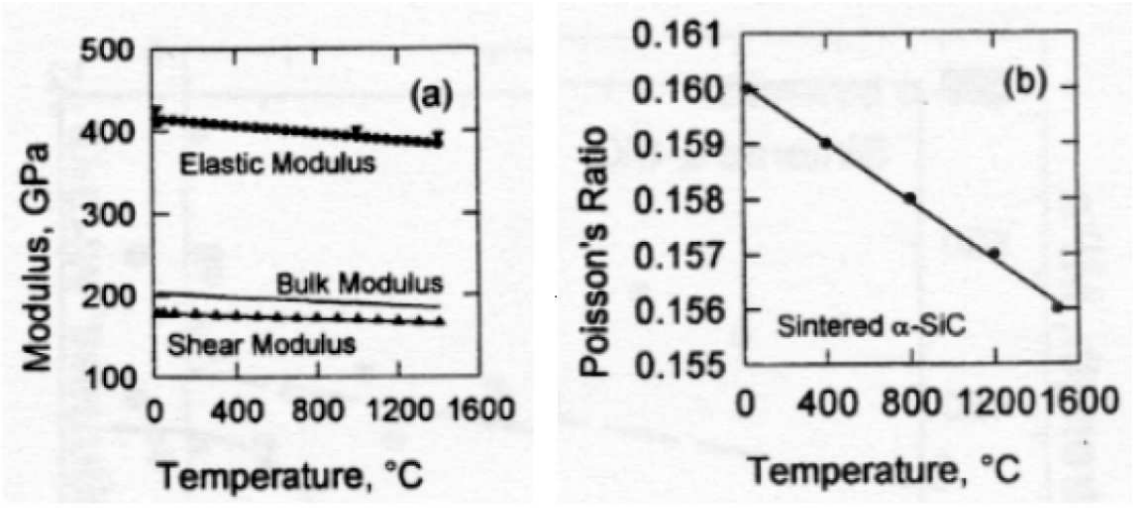


(a) (b)

Figure 3.1. Temperature effect on the elastic properties of SiC [30]

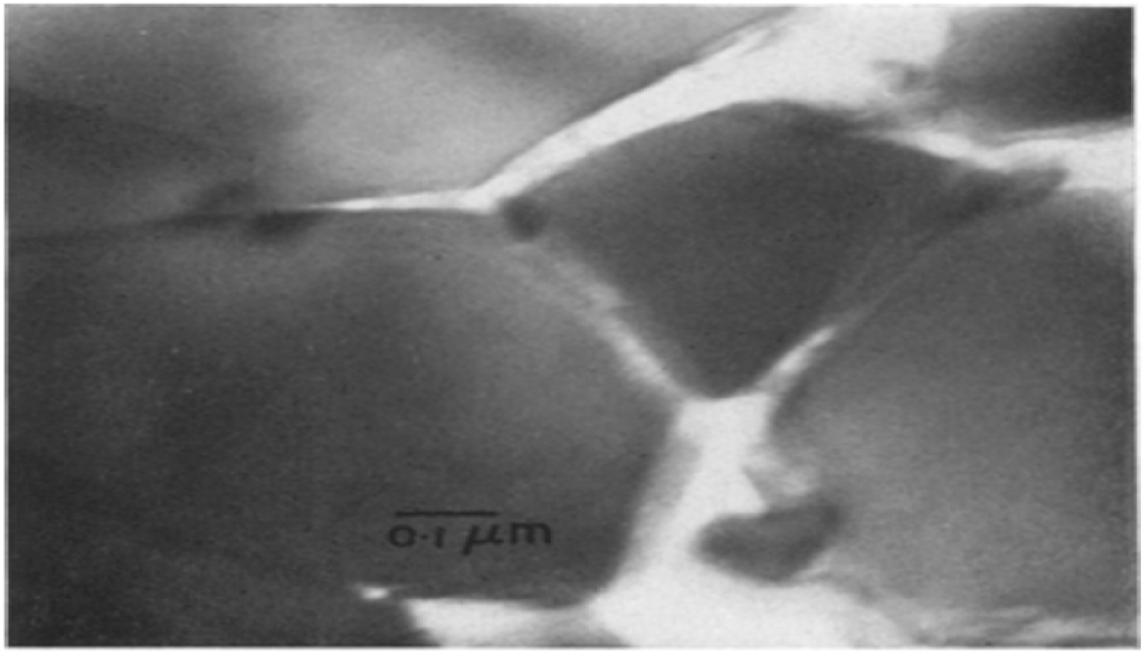


Figure 3.2. Micro-crack growth along grain boundary [35]

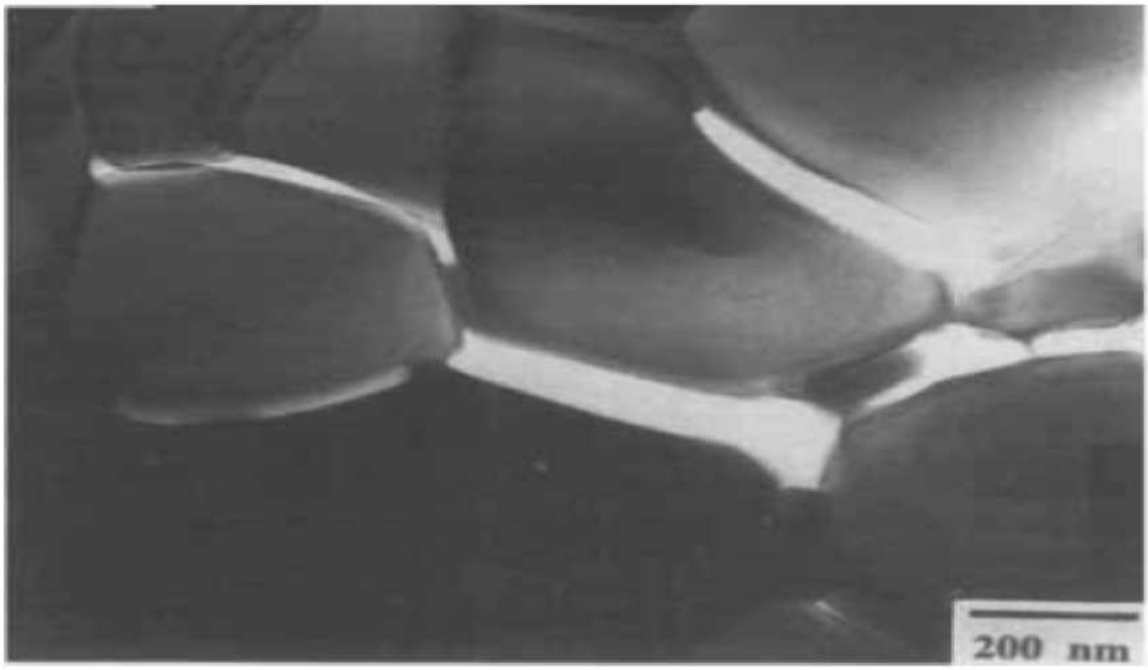


Figure 3.3. GB separation after deformation [36]

microstructure become stronger against fracture. The second phase SiC particles cause a crack bridging effect.

To verify the significance of SiC particles along the grain boundaries, a FEA simulation is carried out using the same CA lattice model. An average from 10 readings is taken from the models having SiC particles and the other one without SiC particles along the grain boundaries. The model with SiC particles in the wake of the grain boundaries has an average fracture energy of 42.45 J and the other with no SiC particles along grain boundaries has an average fracture energy of 32.10 J.

### 3.4 $Si_3N_4$ & SiC properties

Kusunose [37] studied the high-temperature mechanical properties of $Si_3N_4$/BN nanocomposites. The Youngs modulus of the nanocomposite increases gradually maintaining its hardness and strength even at elevated temperatures of 1400°C. The

fracture strength of $Si_3N_4$/BN however decreases at elevated temperatures but the rate is small compared to monolithic $Si_3N_4$.

The grain boundary sliding phenomenon was observed to be a critical factor for the high temperature fracture strength of $Si_3N_4$/BN. The nano sized h-BN particles have excellent high temperatures which were placed along the grains which in turn helped in strengthening these grain boundaries and increasing the strength of the composite [38]. The grain boundaries were thus strengthened by the dispersion of nano sized h-BN particles by chemical processing.

Nihara [39] experimented by embedding nanoparticles (20-300 nm) within the grains and also along the grain boundaries. It was found that along with fracture strength and toughness, even the creep properties were retained because of these dispersed nano sized particles. The properties of these nanocomposites were then compared to monolithic ceramics and the property retention in nanocomposites was therefore attributed to the second phase nanoparticles.

Weimer and Bordia [40] investigated $Si_3N_4$-SiC nanocomposites with aluminum oxide compositions. Their studies concluded that there was 10% improvement in strength in the composite with 5-10% decrease in grain size. But there was a slight decrease in the fracture strength of these composites with the decrease in the grain size.

There are large property variations that have been reported by different researches in the past. These large variations are mainly attributed to the factors like the sample size which is being used for testing, its morphology and also the testing (3 pt. vs. 4 pt.) techniques used. But the critical discrepancy is always found the effect of the dispersed particles on the fracture toughness and strength of the composites which is invariably difficult to test through physical experiments.

A comprehensive study is needed on the effect of the dispersed particles on the mechanical behavior of the composites. A methodical investigation is needed to study the changes in the behavior of the $Si_3N_4$-SiC composite structures due to inclusions of different volume fractions of SiC particles and also its size. These experimental

based studies have not been carried out to find the fracture strength and toughness with variations in the size and volume of SiC particles in the matrix of silicon nitride grains [40].

A small amount of plastic deformation was identified for silicon nitride because of the dislocation motion in the reaction bonded grain boundaries at 1400°C. But at most only "microplastic" deformation is achieved, which is controlled by the "interface reaction" process which depends either on the transfer of matter through the glassy phase or on the mobility of GB-dislocations [29].

Hardness test was carried out on polycrystalline silicon. Initial yield for SiC was taken to be 11.82 GPa based on a proposed value of H/2.2 [41]. Based on initial yield and the Young's modulus test values effective plastic strain values were calculated for SiC at both the temperatures using the relation $\frac{\theta_0}{E}$.

The elastic and plastic properties used for all the three phases are shown in the table material properties at 20°C.

Table 3.1. Material and Mechanical properties at 25°C [15, 42–49]

| **MATERIAL** | **YOUNGS** MODULUS | **POISSON** RATIO | **YIELD** STRESS | **PLASTIC** STRAIN |
|---|---|---|---|---|
| $Si_3N_4$ | 210 GPa | 0.22 | 9.8 GPa | 0.01 |
| SiC | 450 GPa | 0.16 | 14 GPa | 0.02 |
| Grain Boundaries | 190 GPa | 0.22 | 5 GPa | 0.008 |

## 3.5 Methodology of Materials Design

To find the optimal fracture energy of this composite material a 2D model is developed for analysis and optimization. The 2D model which is created using the cellular automation lattice model uses physically based rules and provides a simpler physical realization of folding on a regular lattice in 2D.A finite element fixed mesh is created

Table 3.2. Material and Mechanical properties at 1400°C [15, 42–49]

| **MATERIAL** | **YOUNGS** MODULUS | **POISSON** RATIO | **YIELD** STRESS | **PLASTIC** STRAIN |
|---|---|---|---|---|
| $Si_3N_4$ | 200 GPa | 0.18 | 11.8 GPa | 0.02 |
| SiC | 380 GPa | 0.15 | 16 GPa | 0.05 |
| Grain Boundaries | 170 GPa | 0.17 | 7 GPa | 0.0017 |

using a one to one pixel to element correspondence in LS-Dyna for the non-linear dynamic fracture analysis. The uncertainties in the model are quantified using the Monte Carlo simulation [50]. The optimization is carried out using a surrogate model instead of high fidelity time consuming Finite Element Model. A surrogate model is developed using the radial basis function which helps in reducing the optimization time. So the "high fidelity" 2D Finite Element Model guides the "low fidelity" model towards the optimal design only to make significant savings in time. The radial basis model is not based on true physics.

### 3.5.1 Model for High Fidelity Analysis

A 2D finite element model formed by creating a fixed mesh from the lattice model is used for the high fidelity analysis.

The Figure 3.4 illustrates the composite model analyzed in this research. The second phase(blue) are the second phase SiC particles whose number and size along the grain boundaries(green) has an impact on the fracture energy of this model.

A dynamic non-linear fracture analysis is performed on this Finite Element Model which has a fine resolution of 50 nanometers.

The problem is to design a microstructure having high fracture energy having the constraints of size of the second phase SiC particles of less than or equal to 400 nanometers (i.e 8 pixel radius) and its number to be less than or equal to 15.Therefore

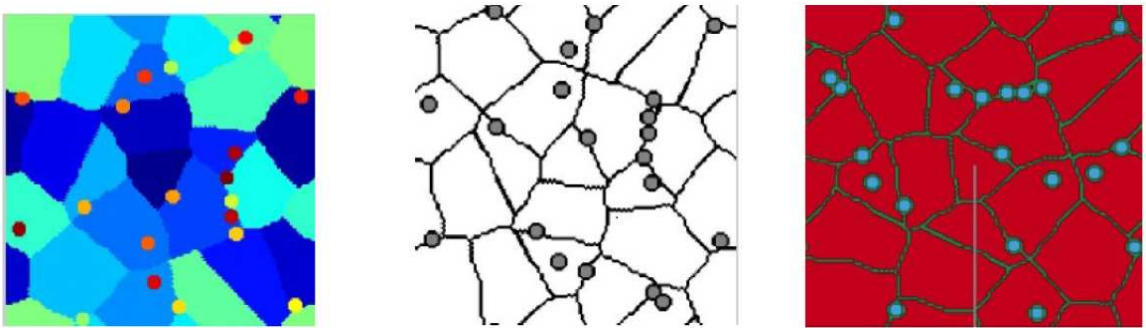

Figure 3.4. 2D Microstructure generation (left), identification of three phases $Si_3N_4$, SiC, and GB (center), and FEA model generation in LS-Dyna (right).

the two design variables are (1) the size of the Silicon Carbide particles and (2) the number of Silicon Carbide particles.

### Explicit FEA using LS-Dyna

Consider the system of $2^{nd}$ order differential equations that govern a discretized structure

$$M\ddot{x}(t) + C\dot{x}(t) + Kx(t) = F(t) \tag{3.2}$$

where $M$ is the mass matrix, $C$ is the damping matrix, $K$ is the stiffness matrix and $\ddot{x}(t)$, $\dot{x}(t)$, $x(t)$ are the vectors of acceleration, velocity, and displacement (respectively) for the nodal locations at any given time $t$. $F(t)$ is the vector of external forces applied to the structure. Solving for acceleration, equation 3-4 becomes

$$\ddot{x}(t) = M^{-1}(F(t) + F_s(t)) \tag{3.3}$$

where $F_s(t)$ is the vector of internal structural forces. In fracture analysis the crack growth pattern is highly time dependent and also the failure occurs in the plastic phase

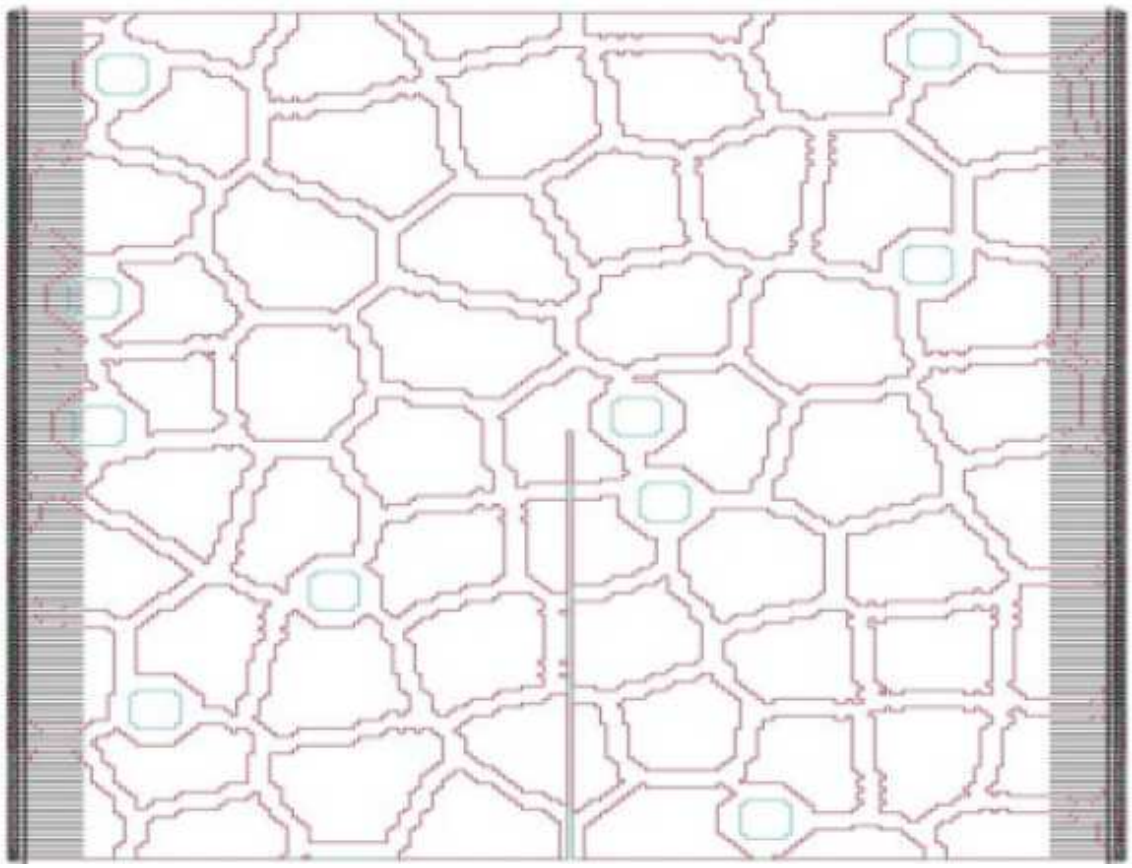

Figure 3.5. Boundary Conditions of the Finite Element Model

of the material. One method for solving such highly non-linear problems is to use an explicit finite element method.

The terms implicit and explicit refer to time integration algorithms. An Explicit FEA analysis utilizes an incremental procedure to solve for nodal dynamics. At the end of each increment, it updates the stiffness matrix based on geometry changes (if applicable) and material changes (if applicable). Then a new stiffness matrix is constructed and the next increment of load (or displacement) is applied to the system. The purpose for this explicit approach is that if the increments are small enough, then the results will be accurate. One problem with this method is that the time increment must be very small for a high level of accuracy and thus the simulation

can be extremely computationally expensive. If the time increment is too large, the solution tends to drift from the correct solution.

### 3.6 Fracture Calculation

While performing finite element analysis the sample is assumed to be defect free. But to incorporate the actual defects in the microstructure, a fictitious crack model is used [16] for the finite element . The stress intensity factor is the parameter for fracture mechanics used in a fictitious crack model. The analytical and experimental methods both have been have extensively being used in the past century to find the fracture behavior of these complex composite materials. The ideal geometries have always been used for analytical and experimental methods to calculate their fracture strength [51] and for the complex geometries numerical methods has been the source to calculate its fracture strength [52, 53]. The LS-Dyna model used for performing the fracture analysis is Material number 81 called as the $*MAT\_PLASTICITY\_WITH\_DAMAGE$.

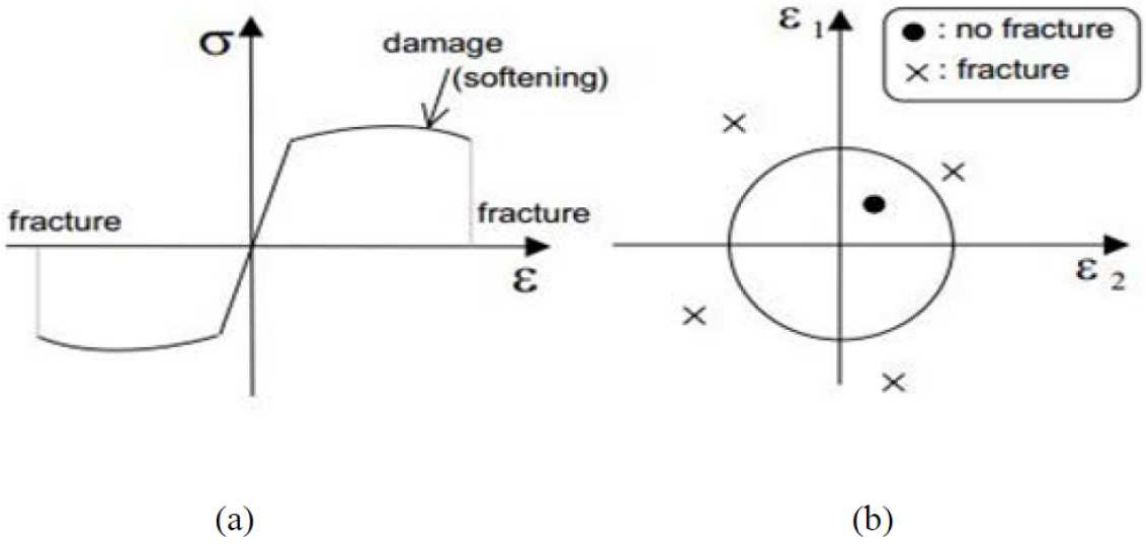


Figure 3.6. Figure (a)Damage Characteristic (b)Fracture criteria [54]

This material model has Isotropic damage and fracture characteristic and its uniaxial stress-strain curve is completely symmetric about an origin. Therefore, damage and fracture occur in tensional and compressive regions. The constitutive properties of the damaged model are obtained from the undamaged material properties. The amount of damage evolved is constituted by the constant $\omega$, which varies from zero if no damage has occurred to unity for complete rupture. For uniaxial loading, the nominal stress in the damaged material is given by

$$\sigma_{nomial} = \frac{\rho}{A}$$

where $\rho$ is the applied load and A is the surface area. The true stress is given by

$$\sigma_{true} = \frac{\rho}{A - A_{loss}}$$

where $A_loss$ is the void area. The damage variable can be defined as $0\omega1$. In model damage is defined in terms of plastic strain after the failure strain is exceeded:

$$\omega = \frac{\varepsilon^p_{eff} - \varepsilon^p_{failure}}{\varepsilon^p_{rupture} - \varepsilon^p_{failure}} \quad if\ \varepsilon^p_{failure} \leq \varepsilon^p_{eff} \leq \varepsilon^p_{rupture} \tag{3.4}$$

After exceeding the failure strain softening begins and continues until rupture strain is reached.

## 3.7 Fracture Analysis of Composite Materials

The main application of the $Si_3N_4$-SiC nanocomposite is in the aerospace industry. Hence the material must have sufficient fracture toughness so that a noticeable crack can be detected before failure. The toughness of the composites depends on the volume fractions of inter and intragranular SiC dispersions, and controlling these fractions precisely is challenging. Ohji [55] proposed a particle-bridge mechanism, whereby crack face shielding results when nano-size particles bridge the crack surfaces.

The SiC particles act as the toughening mechanisms in the composite material because they are mainly responsible for crack deflection and crack impediment.

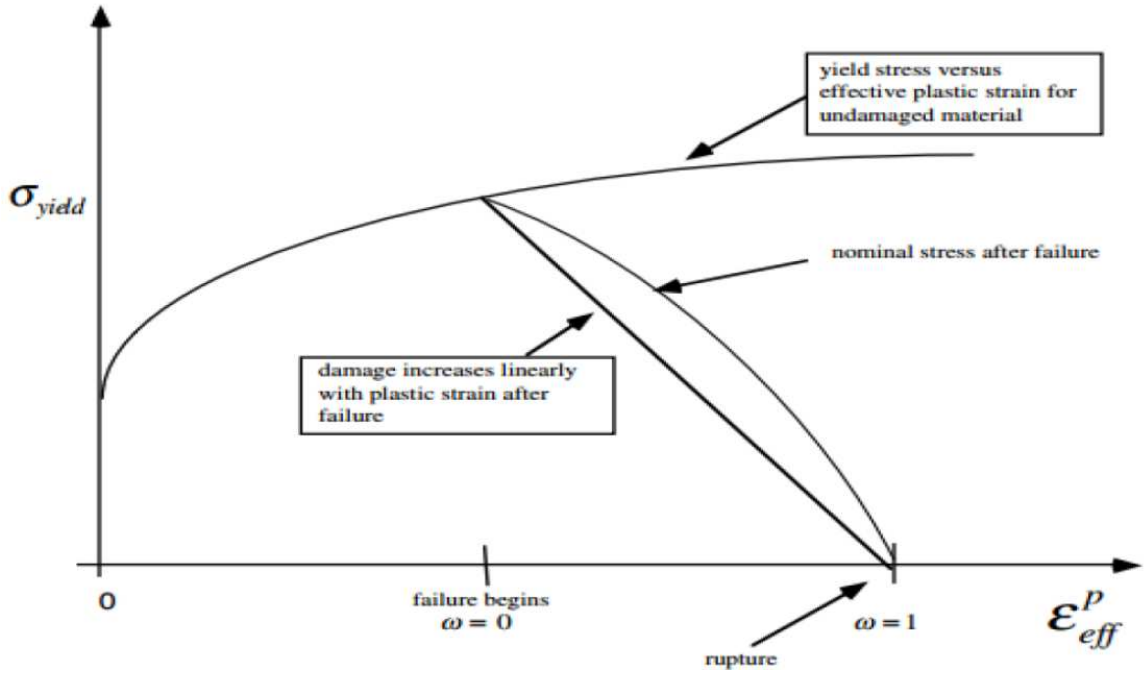


Figure 3.7. Figure. Stress-Strain behavior when damage is included

The average fracture energy of the intergranular structure was found to be 44.68J with a standard deviation of 3.49 while that for a structure having both dispersions was 36.47J with a deviation of 3.12 from 8 readings respectively. Both the structures have 15 SiC particles .Thus, the analysis show that SiC particles along the grain boundaries have significant impact on its fracture energy. Hence the number and size of intergranular SiC particles is chosen as our design variables for finding the morphology with the highest fracture energy.

### 3.8 Microstructural Randomness

With a fixed given set of input parameters different models having the same structural properties but different topologies are generated as the microstructure generation is based on randomness.

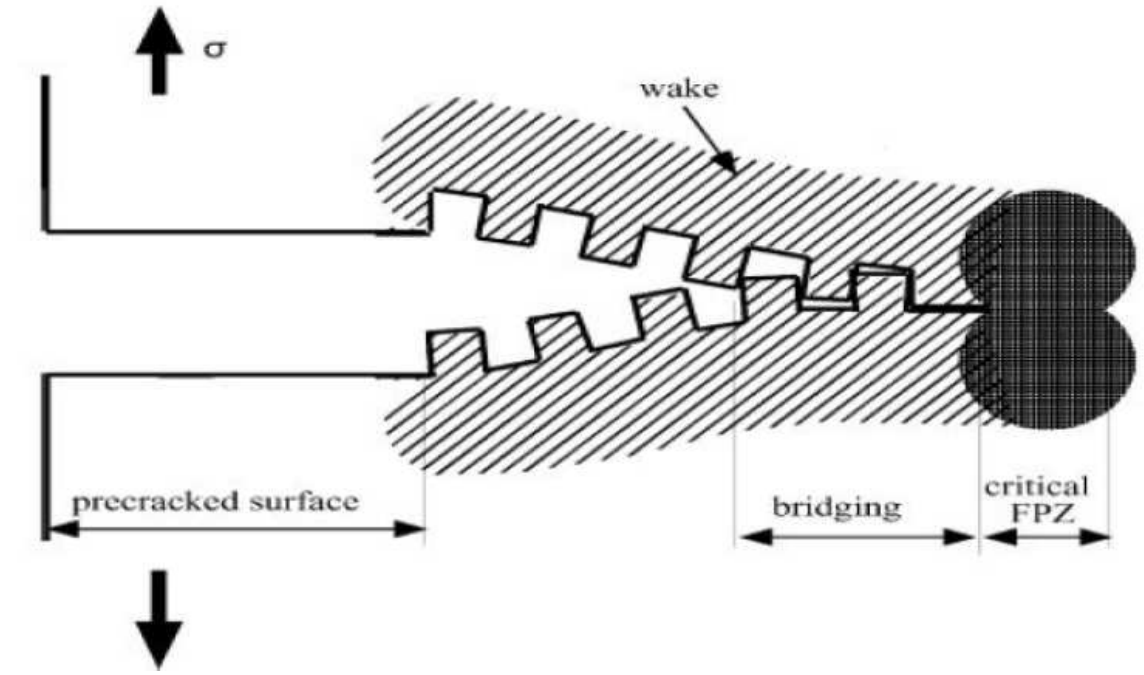


Figure 3.8. Schematic diagram of fracture frontal process zone


Figure 3.9. (A) Intergranular Structure (B) Inter+Intragranular Structure

This formulation goes hand in hand with the actual physical material testing methods because every physical composite having the same parameters is bound to have different topologies.

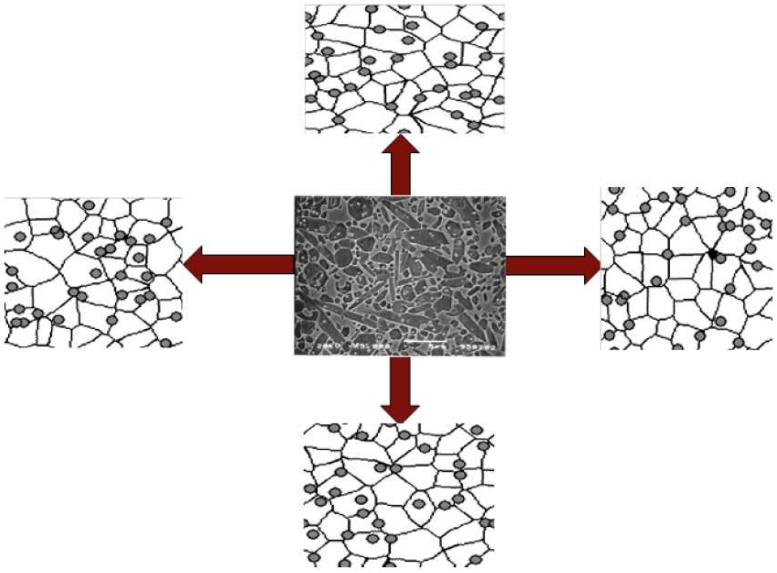

Figure 3.10. Four different lattice models with the same input parameters

But even though they have the same parameters these models are bound to have different fracture patterns and hence different fracture energies.

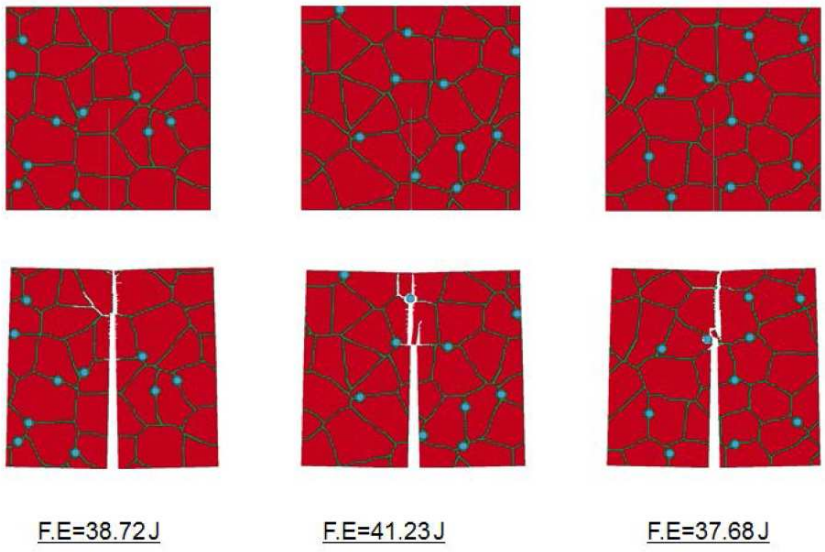


Figure 3.11. Three models of 1010 micrometers with same input parameters but different fracture energies at room temperature

Along with the morphology, the topology of the composite material also plays an important role while determining its fracture toughness.

# 4. DESIGN OPTIMIZATION METHODS

These material design optimization techniques are iterative design based and are computationally very expensive. Therefore, to impregnate these expensive material design cycles in an iterative manner for optimization an efficient design technique is needed. Qian et al. [56], and Osio worked on building surrogate models with good accuracy. But this work primarily focused on adapting the surrogate model technique for decreasing the material design optimization time. Mejía-Rodríguez et al. [50] presented a material design tool based on the variable fidelity model management framework. In this research the high fidelity simulations are used in the algorithm only to obtain the low fidelity simulation results in the accurate range. Response surfaces are generated in Successive approximate optimization (SAO) algorithms to conduct optimization on an inexpensive surrogate model which efficiently reduce the optimization time [57].

In the field of mathematical modeling, a radial basis function network is an artificial neural network that uses radial basis functions as activation functions. The output of the network is a linear combination of radial basis functions of the inputs and neuron parameters. Radial basis function networks have many uses, including function approximation, time series prediction, classification, and system control [58]. The use of radial basis function was proved to be universal approximation [59].This function could therefore successfully used as a surrogate model in expensive computational problems [60].

A Kriging model approach by adopted by Timothy [61] as alternatives to second-order polynomial response surfaces for constructing global approximations for use in a real aerospace engineering application, namely, the design of an aerospike nozzle. The Kriging model is similar to Radial Basis Function except that it combines localized departures or deviations in addition to the global model [62].

In this design process we are using the 2D finite element model as the high fidelity model and the low fidelity model is a surrogate model based on the radial basis function. The low fidelity model neglects the important physics involved in the composite material design hence it is much cheaper to evaluate compared to the expensive high fidelity 2D model.

This section deals with the design optimization algorithms and methods introduced in the earlier sections for material design, that are used in material design effectively to reduce the design cycle time.

## 4.1 Surrogate Model Management Materials Design

High fidelity models are expensive to perform the entire design optimization. Hence low fidelity models are used to drive the expensive high fidelity models towards convergence in a shorter period of time. Higher fidelity models are mostly used in the algorithm to get the accuracy of the results in the latter stage. Accurate high fidelity models are expensive to carry the entire optimization process on [18]. The optimization is carried mostly on the surrogate models and then the high fidelity models are used to refine the accuracy of the design and optimality [63].

## 4.2 Surrogate Model Optimization Algorithm

The reason to use the surrogate model is to lessen the function calls of the high fidelity model. The framework is designed as follows: At the starting point $'x0'$ the objective function is evaluated using both high fidelity $f_{high}(x0)$ and surrogate functions $f_{surrogate}(x0)$.The objective function for the optimization problem is to maximize the fracture energy of the given composite material. The design variables are the size and the number of SiC particles to obtain the most suitable morphology with maximum fracture energy.

Starting point:

$$x0 \in R^n$$

The standard non-linear optimization problem can be written as:

Find:

X=[x1,x2]

x1: Number of inter-granular SiC grains

x2: Size of Intra-granular SiC

Maximize

F= Total Fracture Energy

$f_1$ = fracture energy at 25°C

$f_2$ = fracture energy at 1400°C

$\omega$ = weights for distributing the fracture energy values at temperature 25°Cand 1400°C

$\alpha$ = weights for distributing the fracture energy values of the mean and the ratio of standard deviation to mean

Where

$$FX = \omega F_1(x_1, x_2) + (1 - \omega)F_2(x_1, x_2) \tag{4.1}$$

$$F_1(x_1, x_2) = -\alpha * meanf_1 + (1 - \alpha)\frac{std(f_1)}{mean(f_1)} \tag{4.2}$$

$$F_2(x_1, x_2) = -\alpha * meanf_2 + (1 - \alpha)\frac{std(f_2)}{mean(f_2)} \tag{4.3}$$

At $T_1 = 30$°C

$T_2 = 1400$°C

Subject to

$$0 \leq x_1 \leq 15$$

$$1 \leq x_2 \leq 8$$

The fracture energy is found at room temperature (f1) and also at 1400°C(f2).The calculation of fracture energy can either be calculated by using the entire design space or the high fidelity analysis or by using sampling points of the radial basis model.

### 4.2.1 Design of Experiments

The design of experiment is a set of point's setup for sampling. The goodness of the designs depends on the number of samples which is severely limited by the computational time of each sample. As the design variables are deterministic, the set of sampling points are chosen to effectively cover the entire design space uniformly without hampering the computational cost. The uniformity is obtained by maximizing the distance between the points. Examples of these methodologies are Latin Hypercube sampling and orthogonal arrays. [64]. Latin Hypercube methods have been proposed because of its efficiency.

#### Latin Hypercube Sampling

A stratified sampling approach is chosen by distributing a set of points in the design space by $1/N_s$ distance. The sampling approach samples all the spaces in the given design equally depending on the number of points 'k' [65].

By changing the relation between the points and uniformity, different sets of sampling points can be obtained.

#### Optimal Latin Hypercube Sampling

Johnson, Moore, and Ylvisaker [66] proposed the maximim distance criterion, which maximizes the minimum inter-site distance. Morris and Mitchell [67] applied this criterion to the class of LHDs to nd the optimal LHD. Because there are

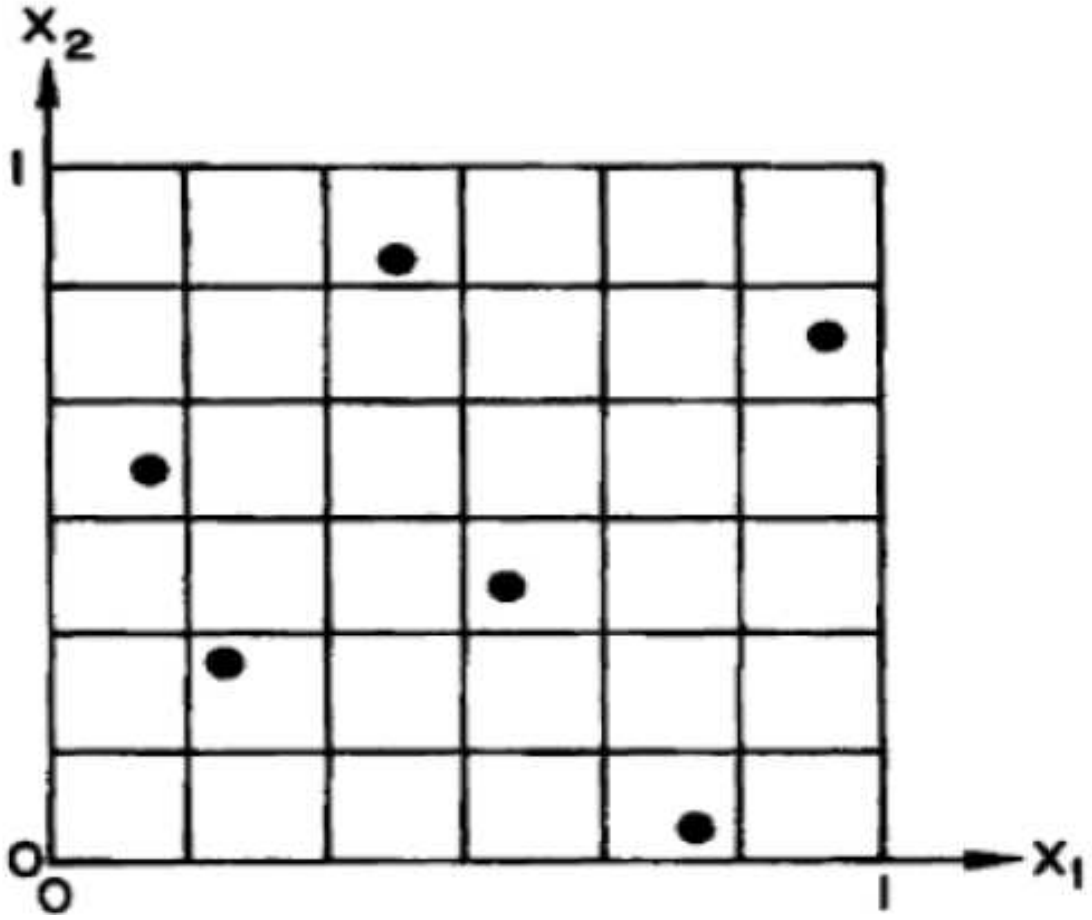


Figure 4.1. A Latin Hypercube Design with $N_s = 6$ and $N_{dv} = 2$ for X uniformly distributed among unit square.

many designs that maximize the minimum inter-site distance, they proposed an extended denition of the maximin criterion. A family of designs defining a distance list $(D_1, D_2, D_3 D_m)$ in which the elements are the distinct values of inter-site distances, sorted from the smallest to the largest for a given LHD. Let $J_i$ be the number of pairs of sites in the design separated by $D_i$.

The family of functions indexed by $p$ is given as

$$\phi_p = (\sum_{i=1}^{m} J_i D_i^{-p})^{1/p} \tag{4.4}$$

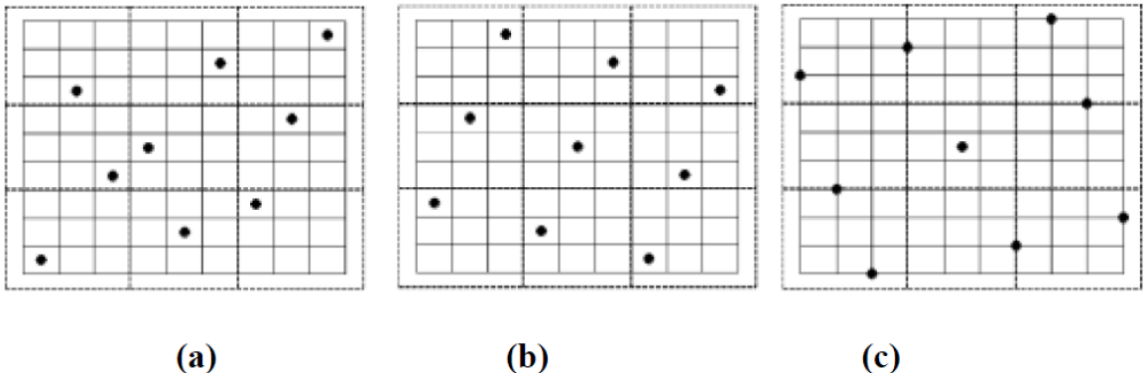


Figure 4.2. LHS designs with significant increase in terms of uniformity from (a) to (c).

where $J_i$ is the number of pairs of sites in the design separated by $D_i$.

The design that minimizes $\phi_p$ is called the maximin design [68]. This design forms the optimal Latin hypercube design (OLHS).

### 4.2.2 Construction of Surrogate Model

There are different ways of constructing a surrogate model with parametric and nonparametric approach. The radial basis function is a non-parametric approach which used data points to create a surrogate model.

#### Radial Basis Function (RBF)

This research explores the implementation of radial basis function networks as a metamodeling technique. It is the intention that the radial basis function network tools can be used to approximate the response of the system normally calculated be means of FEA simulation, and therefor improve computational efficiency.

Radial basis function networks are a type of artificial neural network. An artificial neural network, inspired by the neurobiological workings of the brain, is composed

of an interconnected group of artificial neurons [69]. The network processes information as a relation of connections between these neurons, often referred to as the connectionist approach to computation. A radial basis function (RBF) is simply a function whose value is based on the distance from the origin. In turn, a radial basis network is a neural network that uses RBF functions as the method of neural approximations [70].

A radial basis function network, as shown in, has three layers: an input layer, a hidden layer containing RBF functions, and an output layer. The input layer can be modeled as vector of real numbers $x \in R^n$ and the output is a scalar function of the input vector $\varphi$: $R^n \rightarrow R$. The hidden layer, which contains the RBF functions, is used to approximate the output function expressed as

$$\varphi(x) = \sum_{i-1}^{N} \alpha_i \rho(||x - c_i||) \tag{4.5}$$

where $N$ is the number of neurons, $c_i$ is the center vector for neuron $i$, and $\alpha_i$ is the weight of neuron $i$ in the linear output neuron [71]. The values for $c_i$ and $\alpha_i$ are chosen such that $\varphi(x)$ best fits the data.

Due to the best-fit scheme for the weights, it is necessary to train the neural network with several sets of input data to achieve the desired level of accuracy. As is shown in Figure 4.3, the RBF network takes the set of design variables $d$ as inputs and approximates a value for the system response of interest. LS-DYNA finite element simulations are used to train the network initially through a factorial of the input variables. The optimization problem is then solved and the output is compared to an additional FEA simulation for evaluation of network accuracy. The optimization routine is illustrated in Figure 4.4 . The RBF network implemented here is the function newrbe which exists as part of the Matlab neural toolbox plug-in.This function can produce a network with zero error on training vectors. It is called in the following way: net = newrbe (P, T, SPREAD).

The function newrbe takes matrices of input vectors P and target vectors T, and a spread constant SPREAD for the radial basis layer, and returns a network with

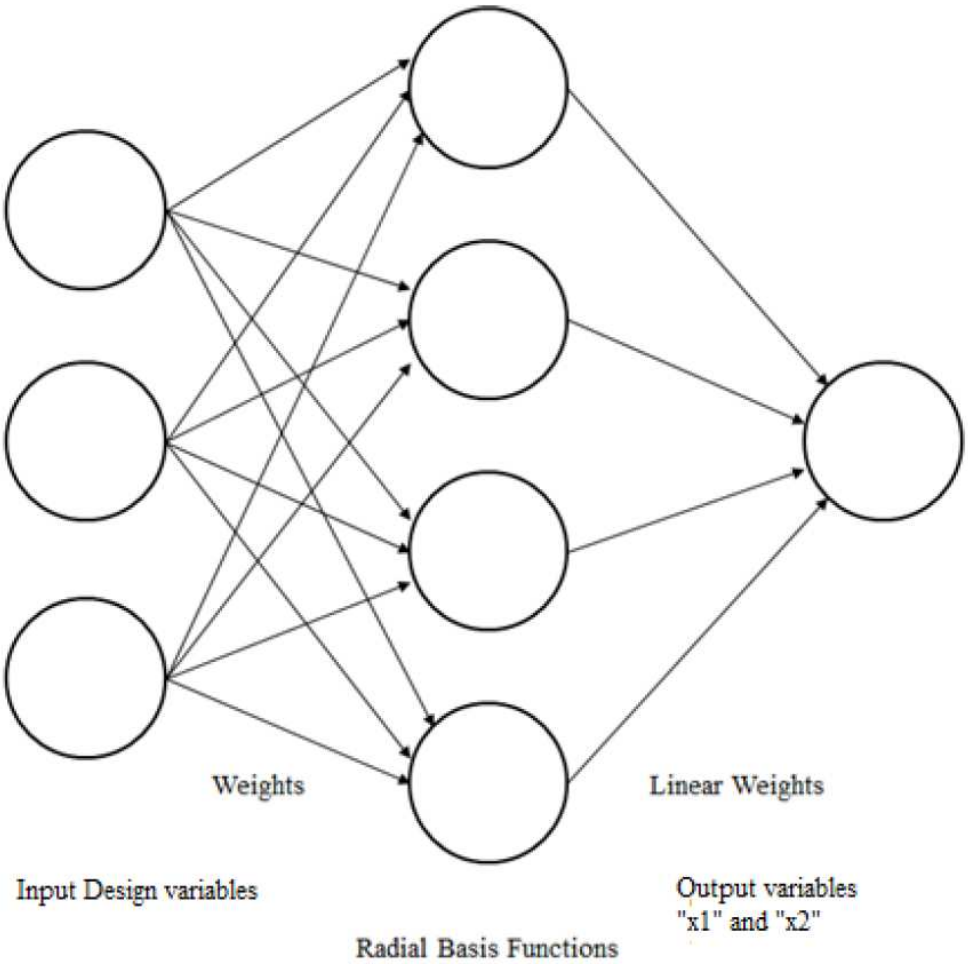


Figure 4.3. Radial basis function architecture [72]

weights and biases such that the outputs are exactly T when the inputs are P. Each bias in the first layer is set to 0.8326/SPREAD. This gives radial basis functions that cross 0.5 at weighted inputs of +/ SPREAD. This determines the width of an area in the input space to which each neuron responds. Hence, the value of SPREAD needs to higher than 1(depending on the function) so that neurons respond strongly to overlapping regions of the input space.

**Optimize Surrogate Model**

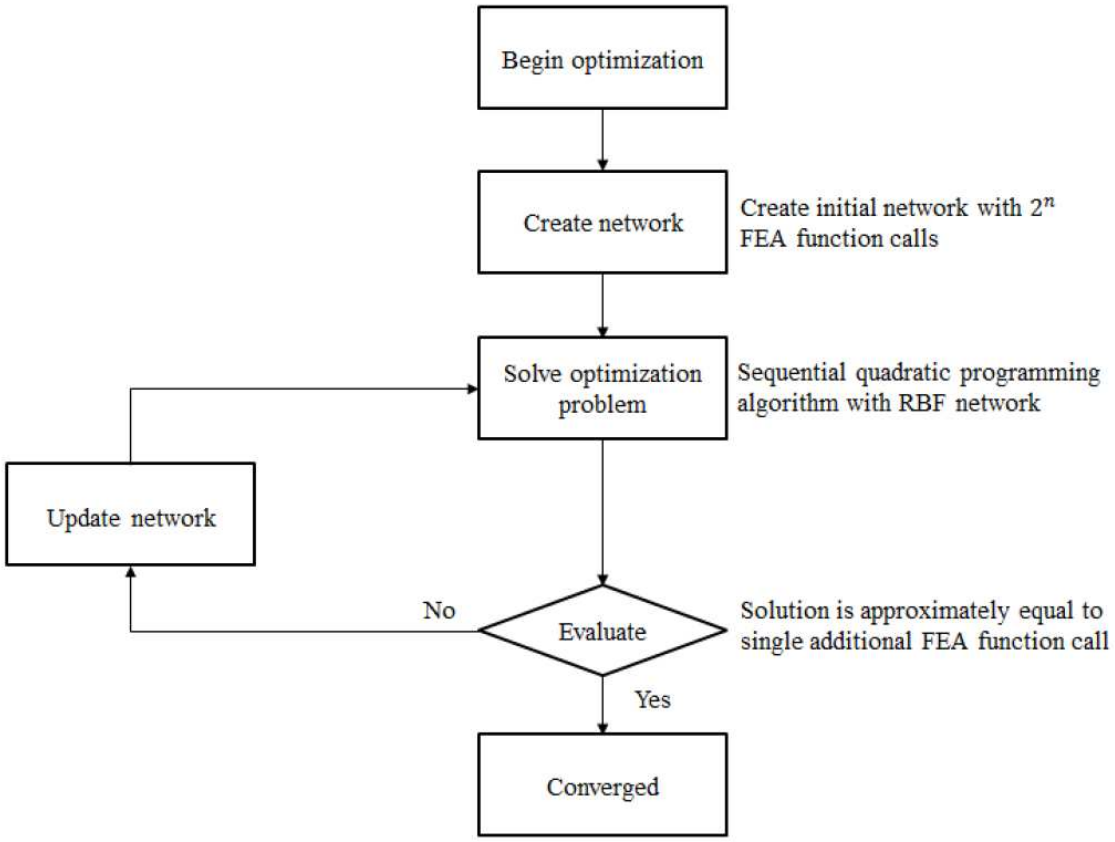


Figure 4.4. Surrogate Model Optimization Framework

**Evaluate new design**

A new point $x_n$ the value taken is of the high fidelity function. If the evaluated function value is within the convergence criteria then the solution is accepted otherwise the evaluated function value is added in the network to create a new RBF for further iterations.

The optimization is carried out using the sequential quadratic algorithm from the Matlab toolbox. The command used in the Matlab program is called the fmincon which solves a quadratic problem at every iteration.

## 4.3 Robust Design Algorithm

A sequential approximate optimization under uncertainty algorithm is applied to find the optimal morphology of the nanocomposite material. Robust Design Method, also called Taguchi Method, was originally developed by Genichi Taguchi [73]. In robust or statistical optimization, a design variable which is the most feasible and efficient is found which minimizes or maximizes the objective function is found.

There is a significant need to apply uncertainty quantification in the area of material optimization due to the errors occurring in design. The quantification of how uncertainty propagates throughout the system is the general goal of such endeavors and is commonly referred to as uncertainty propagation.

Monte Carlo simulation is a well-known method of quantifying the uncertainty and is extensively used in physical and mathematical problems and are most suited to be applied when it is impossible to obtain a closed-form expression or infeasible to apply a deterministic algorithm. Monte Carlo methods (or Monte Carlo experiments) are a broad class of computational algorithms that rely on repeated random sampling to obtain numerical results; i.e., by running simulations many times over in order to calculate those same probabilities heuristically.

This simulation method was introduced in uncertainty quantification of Markov Unreliability Models [74]. When the simulation programs may have deviations associated with input parameters (external uncertainties), as well as internal uncertainties due to the inaccuracies of the simulation tools or system models it is difficult to compromise on the output of the system. These uncertainties will have a great influence on design negotiations between various disciplines and may force designers to

make conservative decisions. Hence this statistical methodology proved to be a good approach to mitigate the effect of uncertainty in simulation based design [75].

### 4.3.1 Uncertainty Quantification of Material Design Model

This method that this research used for optimization is the Monte Carlo method wherein orthogonal arrays are set to evaluate the variations in the design. With the decrease in the number of function calls a trade-off is achieved between the function accuracy and the optimization convergence time. Hence, to reduce the accuracy a multi-objective function with variations of the objective function is also added with the conventional objective function.

The optimization formulation in this investigation takes the form:

Minimize:

Find:

$$x \in R^n$$

Minimize:

$$F(x) = \alpha \hat{f}_p(x) + (1-\alpha) vrt[f_p(x)] \tag{4.6}$$

Subject to:

$$x^L \leq x \leq x^U$$

where :

$f_p(x)$ = fracture energy

defined as:

$$f_p(x) = f(x) + \Omega[R, g(x)]$$

$\Omega$ = summation of variation of fracture energy values and

$$vrt[f_p(x)] = \sqrt{\frac{1}{ns}\sum_{i=1}^{ns}(f_{pi} - \hat{f}_p)^2}$$

In the research of Gu and Renaud [76] the sample designs $i$ in Equation 3-4 are determined by orthogonal arrays for selecting a combination of design variables. In this investigation, there are random errors arising in the microstructure generation simulations so there is no requirement of using orthogonal array technique for quantifying the uncertainty. The variation in results with the same input parameters is the basis of uncertainty quantification, see Figure 4.5.

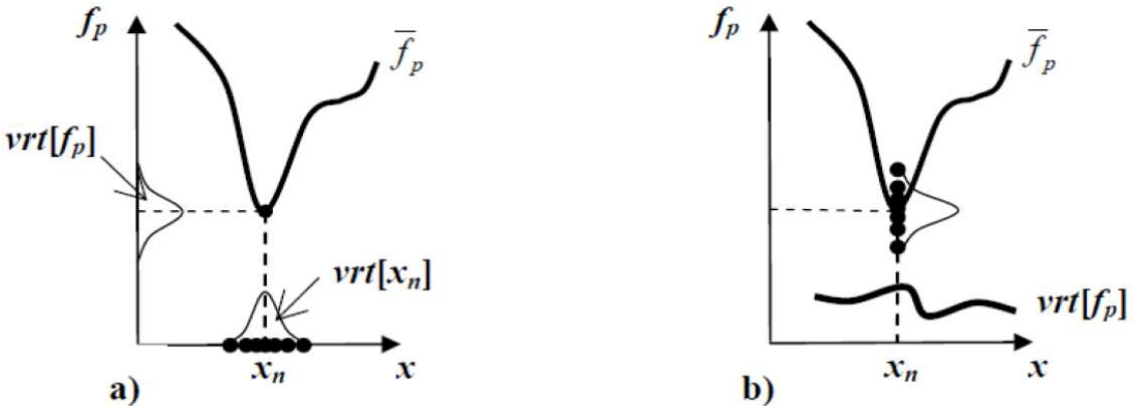


Figure 4.5. a) Input variable non-deterministic b) Function value non-deterministic

### 4.3.2 Quantifying the Response of Non-Deterministic Function

In this research the function fracture energy is a non-deterministic function, caused mainly due to random errors in the microstructural generation simulations [77]. The microstructure is generated based on a random process. The design is repeated 20 times for each design point to quantify the uncertainty [1]. The mean and standard deviation values are obtained from these responses. The mean and standard deviation values obtained are used to create the surrogate models. After 20 simulations the standard deviation of the responses was stabilized and hence it was chosen as a number to quantify the uncertainty.

## 4.4 Verification of Surrogate Model Algorithm

The verification of the Surrogate Model is done using the Rosenbrock function or the banana function. In mathematical optimization, the Rosenbrock function is a non convex function used as a performance test problem for optimization algorithms introduced by Howard H. Rosenbrock in 1960. It is also known as Rosenbrock's valley or Rosenbrock‘s banana function.

The global minimum is inside a long, narrow, parabolic shaped flat valley. To find the valley is trivial. To converge to the global minimum, however, is difficult. The function is defined as:

$$f(x, y) = 100(1 - x^2) + (y - x^2)^2 \tag{4.7}$$

### 4.4.1 Initialization

The optimization of the banana function is carried out in Matlab. The function resembles a parabolic curve. A start point of $[0.5; 0.5]$ is given for SQP algorithm using the $fmincon$ function. The function is also given a lower bound of $[0; 0]$ and an upper bound of $[2.5; 2.5]$.The high fidelity function converges to a value of 0.0000 with the results $[1.0000; 0.9999]$.

### 4.4.2 Design of Experiments

The sampling points are setup using the Optimal Latin Hypercube in ISIGHT. 15 sampling points are chosen between the defined lower and upper bounds. The optimal Latin Hypercube effectively covers the function domain between the defined bounds.

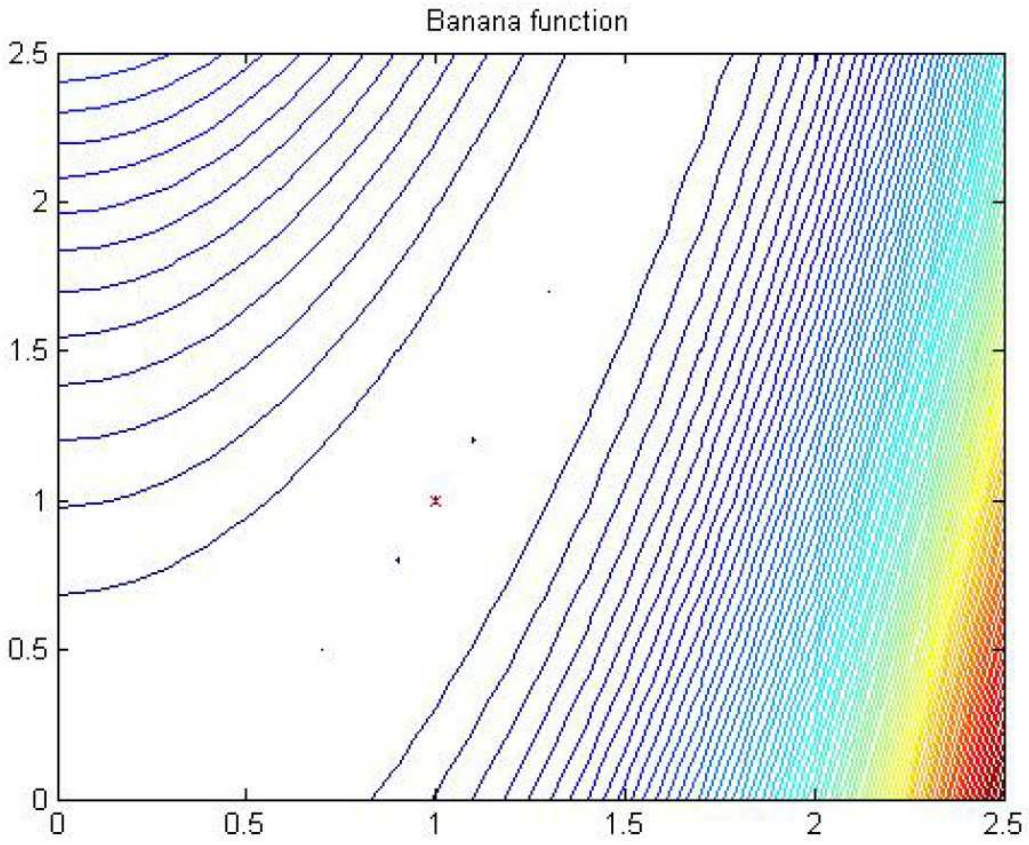


Figure 4.6. Banana Function converged: Banana Function with $[1.0000; 0.9999]$ optimum

### 4.4.3 Construction of the Surrogate Model

The surrogate model is setup using the radial basis function in Matlab. It uses the in-built function "newrbe" for setting up a neural network of the radial basis function. The value of SPREAD is taken based on the judgment with solving the function on trial functions like the banana functions. The value of '3' is chosen as the SPREAD value for this fracture energy function because it invariably gives the best solution based on the results obtained.

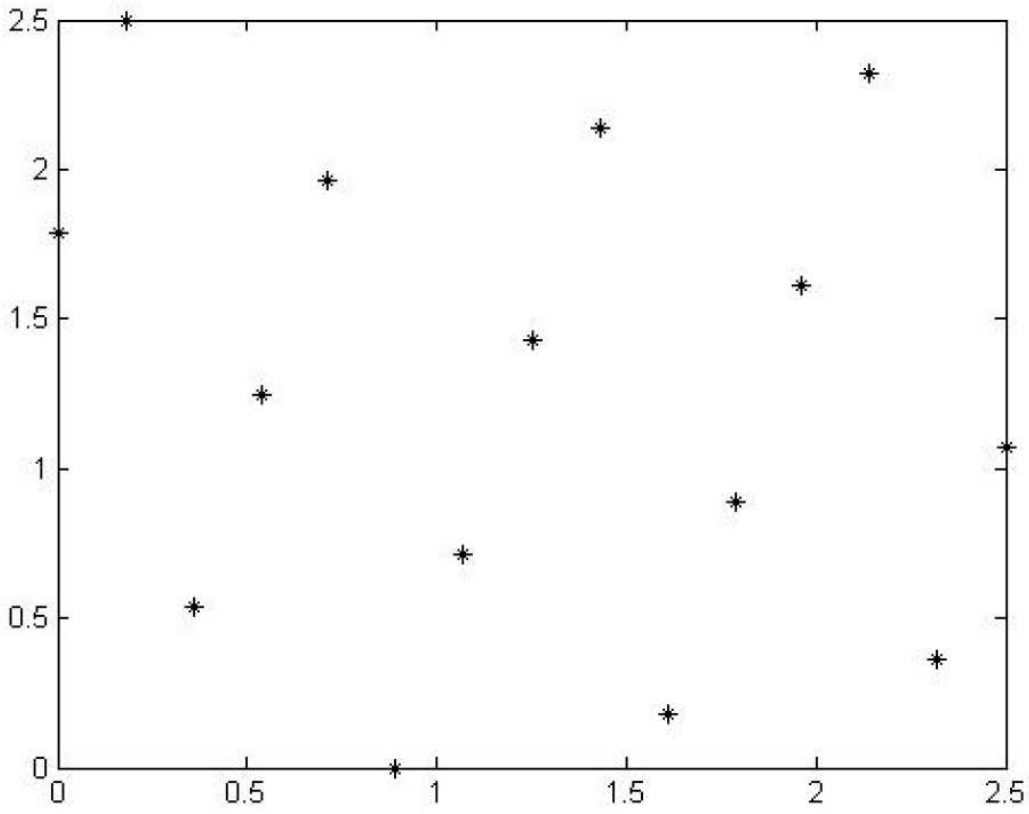


Figure 4.7. Sampling using Optimal Latin Hypercube:15 sampling points between the defined function bounds

### 4.4.4 Surrogate Model Optimization

The optimization based on Surrogate Model based on the Surrogate Model Optimization algorithm is carried out. The results are shown in the following table.

Table 4.1. Convergence obtained using surrogate model optimization on banana function

| Model | x | y | Function calls | Function value |
|---|---|---|---|---|
| High Fidelity | 1.0000 | 0.9999 | 106 | 0.0000 |
| Surrogate | 0.9993 | 1.0005 | 30 | 0.0004 |

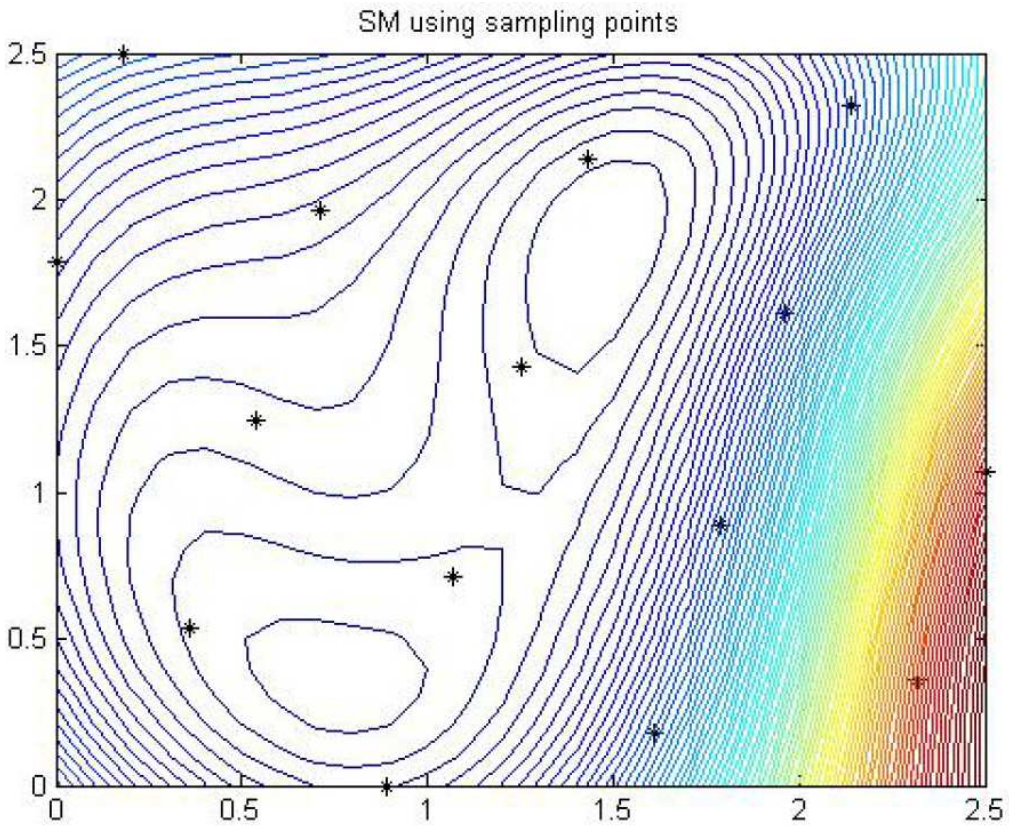


Figure 4.8. Surrogate Model Using Radial Basis Network

## 4.5 Variable Fidelity Algorithm

A low fidelity model (LFM) is added to the algorithm to further reduce the optimization time. The low fidelity model is based on physics but is not accurate as the high fidelity model. The low fidelity model is also compared along with the high fidelity model to the surrogate model result in the convergence criteria. The low fidelity model further reduces the optimization time and high fidelity function calls. The variable fidelity algorithm with lower number of Monte Carlo simulations with that used for the high fidelity model could not implemented in this research because the variations in the values of standard deviations increases with the increase in the

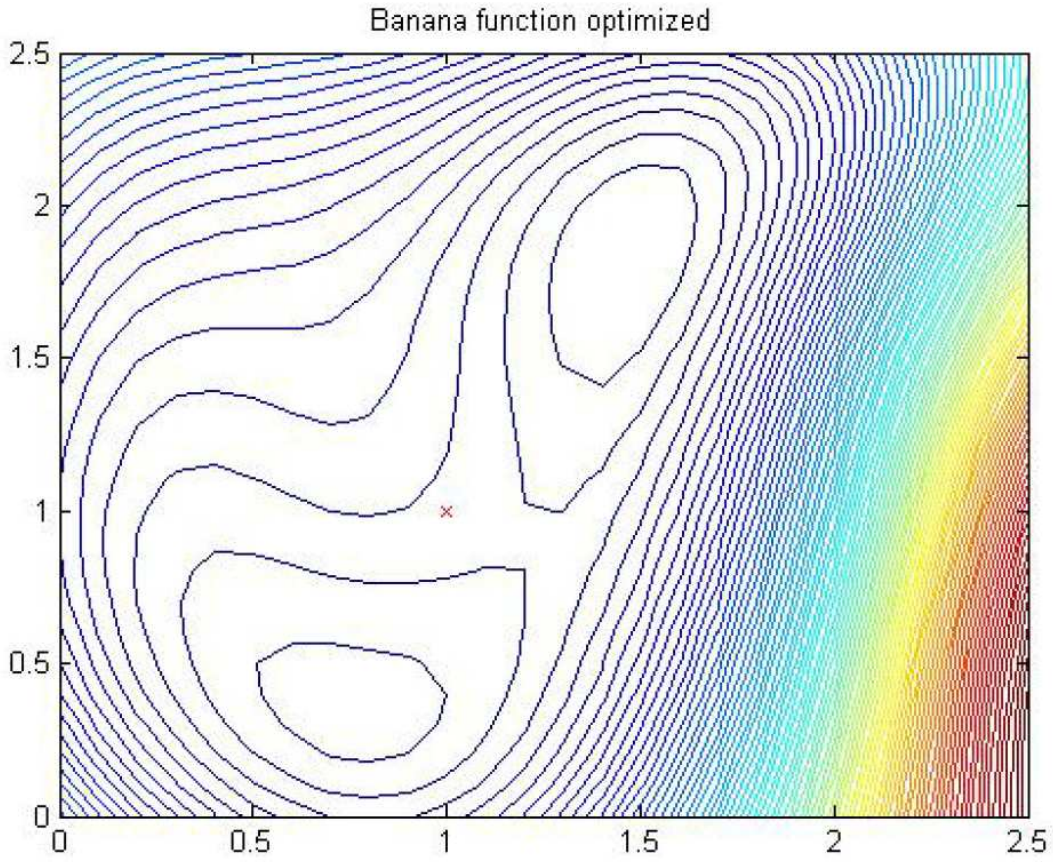


Figure 4.9. Banana function optimized

number and size of SiC phase. The radial basis function would have been inefficient in this case to do an approximation of the low fidelity model.

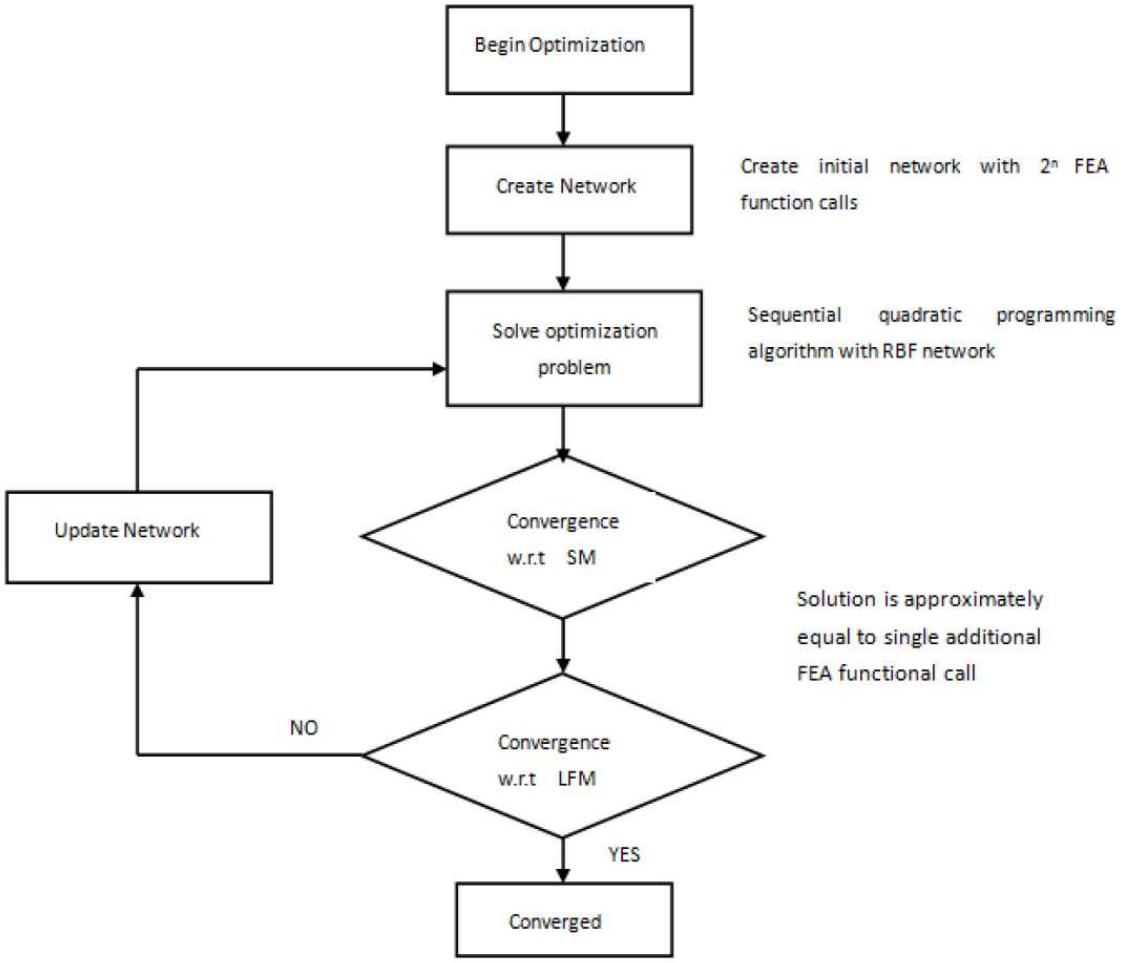


Figure 4.10. Variable Fidelity Algorithm

# 5. COMPOSITE MATERIAL DESIGN RESULTS & SUMMARY

The most optimal morphology of the nanocomposite SiC-$Si_3N_4$ for both low and high temperatures is presented in this chapter. The optimal morphology is predicted by maximizing the fracture energy function at two temperatures: 25°Cand 1400°C. The fracture point is determined by the area under the force-displacement curve by performing tensile tests using the finite element method. The optimization algorithm used is the sequential approximate along with quantifying the uncertainties in finding the optimal morphology of the nanocomposite. The uncertainties arising from the random errors in the model are quantified using the Monte Carlo simulation [1]. The results show that the SiC volume fraction, the number of $Si_3N_4$ grains, grain size distribution of the $Si_3N_4$ grains have significant effects on the fracture energy values. At room temperature (25°C) the preferred material is one with higher $Si_3N_4$ and on the other hand the preference is on the material with higher SiC volume fraction. The results found in this investigation are in conjecture with the findings and results in the literature. This study is overall a systematic methodology in predicting the optimal morphology of the SiC-$Si_3N_4$ ceramic composite which maximizes the fracture energy of the microstructure and at the same time reduces the optimization time. The investigation is performed on the $Si_3N_4$-SiC composite but this methodology can be extended to any composite mateial [1].

## 5.1 Methodology for Materials Design

To implement the proposed material design methodology, a function having equal weights of fracture energy at 25°Cand 1400°Cis maximized with simultaneously quantifying the uncertainties in the model. The microstructural generation input parameters are variable bound along with its size.

### 5.1.1 Design Model

A Finite Element fixed mesh model derived from lattice model in Matlab is chosen for achieving the design objective.

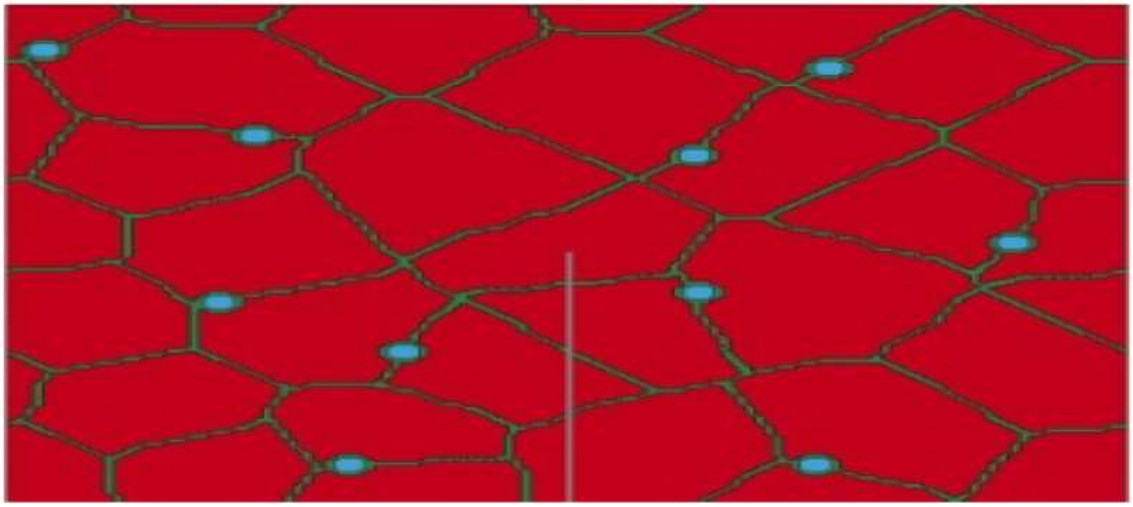

Figure 5.1. Finite Element Model

Choosing a correct sample size for analysis and further for optimization is of utmost importance for getting the correct optimum point in the chosen design methodology. Some researches use a square sample and some use a rectangular sample for fracture analysis [78, 79]. A square sample of $7.5 * 7.5$ micrometers and a rectangular sample of $7.5 * 10$ micrometers are compared with their average fracture energies and standard deviations taking 20 readings each. The resolution of the structure is 20 pixels to one micrometer. Hence, a unit radius of SiC particle represents 0.05 micrometers, i.e. 50 nanometers.

The contour plot of the deviations of the square model shows that the standard deviation increases as the number and size of SiC particles increase. But the contour of a rectangular model is smoother and shows no such rapid increase in standard deviation with change in the SiC particle size and dimension. Although the values of deviation are a bit higher for a rectangular model but the variance is very less if

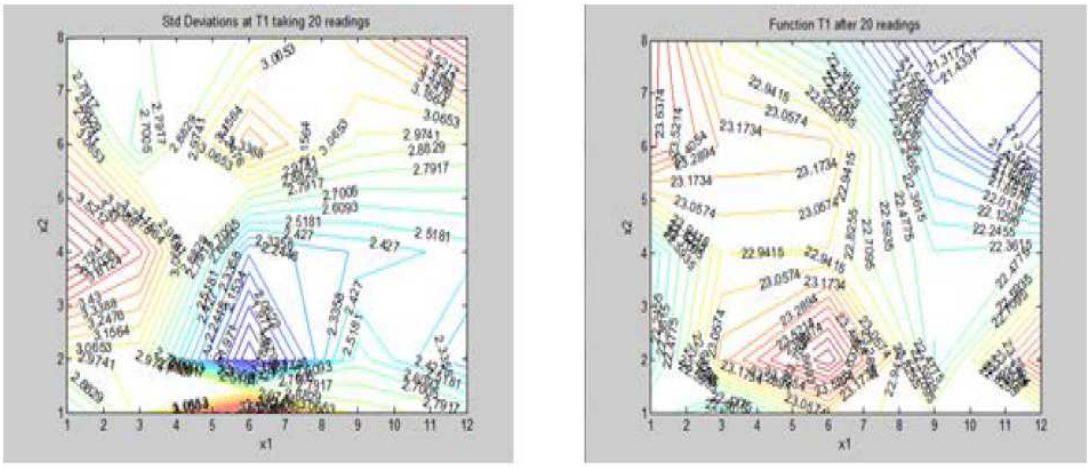


7.5 x 7.5 Micrometers

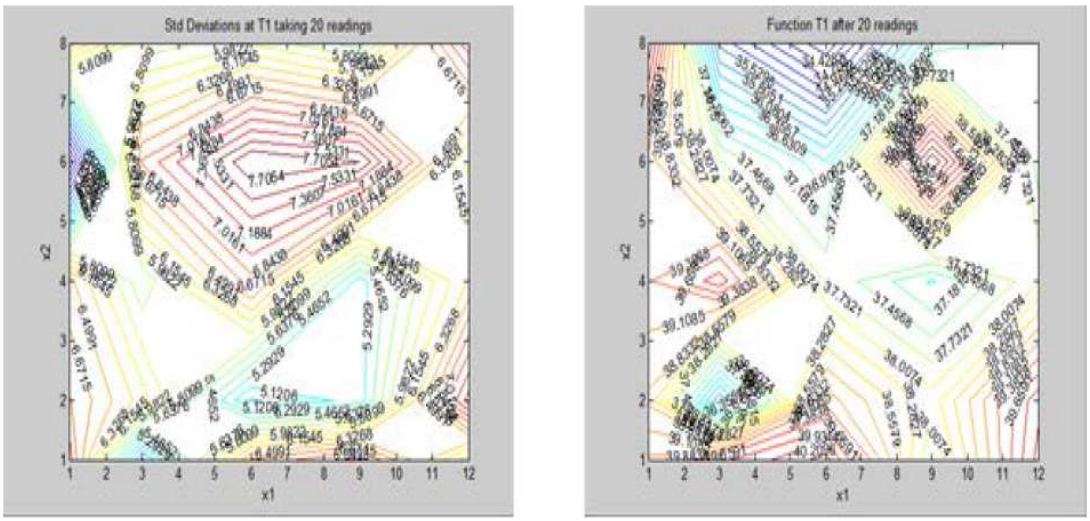


7.5 x 10 Micrometers

Figure 5.2. Standard deviations and fracture energies of a square sample ($7.5 * 7.5$ micrometers) top and Standard deviations and fracture energies of a rectangular sample ($7.5 * 10$ micrometers)

we take into account the values of fracture energies (Figures on the right).Hence, a

rectangular model gives better results and can serve as an ideal model for further investigations. The model size chosen for this research was $6.25 * 12.5$ micrometers.

### 5.1.2 Design Model Objective

The number of silicon nitride grains and the intra-granular SiC particles are chosen as the fixed parameters while achieving the desired design objective.

A filter radius of 2.25 is kept constant for both SiC and $Si_3N_4$ phases in the CA lattice model for all the inputs to obtain a nearly uniform round structure of all the cells. The filter radius for the grain boundaries is 1.25 for achieving a square structure for every pixel. The diameter (or the critical radius distance) is kept constant to be 0.7 throughout all the readings.

Fixed Parameters:

Total $Si_3N_4$ grains = 30;

Intra-granular SiC particles = 0;

Weights: $\alpha = 0.5$ $\omega = 0.5$

Find:

X=[x1,x2]

x1: Number of inter-granular SiC grains

x2: Size of Intra-granular SiC

Maximize

F= Fracture Energy

Where

$$FX = \omega F_1(x_1, x_2) + (1 - \omega)F_2(x_1, x_2) \tag{5.1}$$

$$F_1(x_1, x_2) = -\alpha * meanf_1 + (1 - \alpha)\frac{std(f_1)}{mean(f_1)} \tag{5.2}$$

$$F_2(x_1, x_2) = -\alpha * meanf_2 + (1 - \alpha)\frac{std(f_2)}{mean(f_2)} \tag{5.3}$$

At $T_1 = 30°C$& $T_2 = 1400°C$

Subject to

$$0 \leq x_1 \leq 15$$

$$1 \leq x_2 \leq 8$$

In equation 5-2 $f_1$ represents the fracture energy at temperature $T1$ and $f_2$ represents the fracture energy at temperature $T2$, $std(f_1)$ and $mean(f_2)$ represent the standard and mean deviation of the fracture energies derived from the Monte Carlo method. The parameter $\omega$ is used to distribute the weight of the fracture energies in the equation and  is the parameter used to distribute the weight of the uncertainties to be adopted in the equation. The Matlab function fmincon is used for the optimization [1].

Table 5.1. Material and Mechanical properties at 25°C [15, 42–49]

| **MATERIAL** | **YOUNGS** MODULUS | **POISSON** RATIO | **YIELD** STRESS | **PLASTIC** STRAIN |
|---|---|---|---|---|
| $Si_3N_4$ | 210 GPa | 0.22 | 9.8 GPa | 0.01 |
| SiC | 450 GPa | 0.16 | 14 GPa | 0.02 |
| Grain Boundaries | 190 GPa | 0.22 | 5 GPa | 0.008 |

Finite element simulations give us the result of the area under the force-displacement curve which is nothing but the fracture energy of the material up to the fracture limit. Table 3-1 & Table 3-2 show the elastic material properties for the bulk components of the SiC-$Si_3N_4$ nanocomposite.

The microstructural generation simulations induce uncertainties in the model which in turn generate uncertainties in the finite element analysis. With the same input parameters for the microstructural generation simulation, different models with

Table 5.2. Material and Mechanical properties at 1400°C [15, 42–49]

| **MATERIAL** | **YOUNGS** MODULUS | **POISSON** RATIO | **YIELD** STRESS | **PLASTIC** STRAIN |
|---|---|---|---|---|
| $Si_3N_4$ | 200 GPa | 0.18 | 11.8 GPa | 0.02 |
| SiC | 380 GPa | 0.15 | 16 GPa | 0.05 |
| Grain Boundaries | 170 GPa | 0.17 | 7 GPa | 0.0017 |

variations in its characteristics are generated and therefore fracture energy results with variations are achieved.

The initial surrogate design matrix is setup using the optimal Latin hypercube in Isight.8 sampling points are setup initially for covering the design space effectively. The sample size chosen for this investigation is $6.25 * 12.5$ micrometers. The number of silicon nitride grains is kept constant to be 30 throughout the investigation.

Table 5.3. Design matrix chosen from ISIGHT using OLH sampling method

| X1 | X2 |
|---|---|
| 1 | 1 |
| 2 | 3 |
| 4 | 2 |
| 1 | 4 |
| 5 | 7 |
| 9 | 3 |
| 12 | 4 |
| 15 | 6 |

## 5.2 Results

### 5.2.1 $\omega = 0.5$ and $\alpha = 0.5$

By using $\omega = 0.5$ we use equal distribution of both the temperatures in the equation. By using $\alpha = 0.5$ we take 50% weightage of the uncertainties in the design. Surrogate model is created from the fracture energy responses. Every sample is tested 20 times to quantify the uncertainty. The standard deviations of fracture energies for both the temperatures were around 3.2.

Table 5.4. Results for $\omega = 0.5$ and $\alpha = 0.5$

| | **High Fidelity Model** | **Surrogate Model** |
|---|---|---|
| **Fracture Energy** | 21.551 J | 21.508 J |
| **Number of functions calls** | 5 | 227 |

The optimized result for the above input conditions is as shown in the Figure 5.3. The optimum result obtained is $[10, 3]$.Hence the average size of SiC particles is 600 nanometers.

### 5.2.2 $\omega = 0.5$ and $\alpha = 1$

By using $\alpha = 1$ we do not consider the standard deviations of the fracture energies. Surrogate model is created from the fracture energy responses. Every sample is tested 20 times to quantify the uncertainty [1].

Table 5.5. Results for $\omega = 0.5$ and $\alpha = 1$

| | **High Fidelity Model** | **Surrogate Model** |
|---|---|---|
| **Fracture Energy** | 21.898 J | 22.050 J |
| **Number of functions calls** | 7 | 285 |

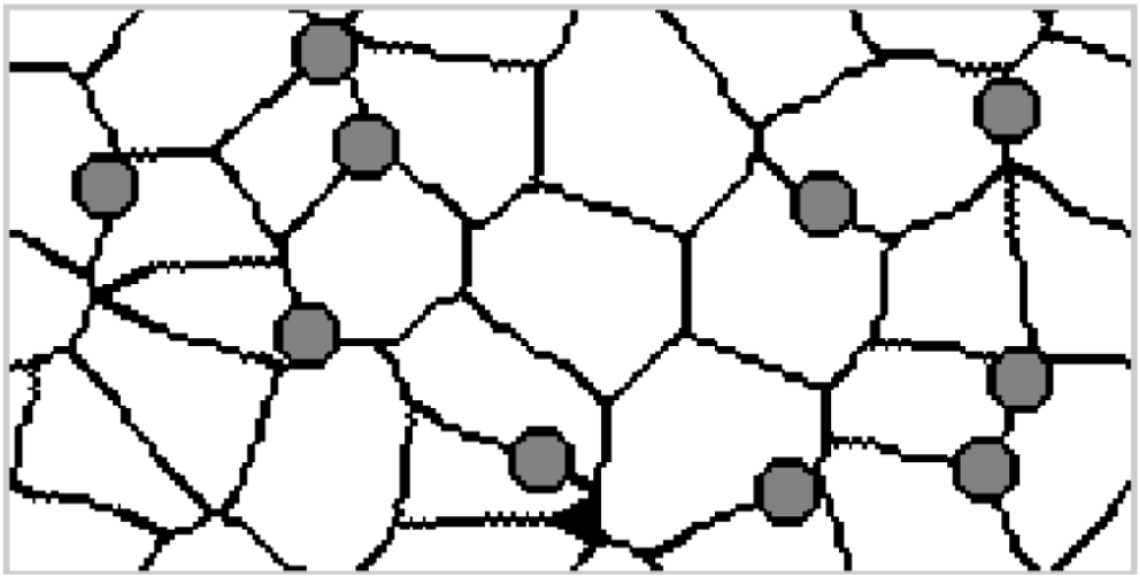

Figure 5.3. Optimal Morphology for input $\omega = 0.5$ and $\alpha = 0.5$

The number of SiC particles and its size is same as shown in the Figure 5.3 but it takes 58 more functions calls to converge to the same solution. Hence, it proves that considering a low fidelity model takes more function calls for the solution to converge.

### 5.2.3 Temperature 1400°Cand $\alpha = 0.5$

By using $\omega = 0$ we consider only the sample for temperature 1400°C. By using $\alpha = 0.5$ we take 50% weightage of the uncertainties in the design. Surrogate model is created from the fracture energy responses. Every sample is tested 20 times to quantify the uncertainty. The standard deviations of fracture energies for both the temperatures were around 2.4.

The optimized result is as shown in the Figure 5.4.The optimum result obtained is $[5, 7]$.Hence the average size of the SiC particles is 1000 nanometers.

Table 5.6. Results for Temperature 1400°Cand $\alpha = 0.5$

| | **High Fidelity Model** | **Surrogate Model** |
|---|---|---|
| **Fracture Energy** | 24.600 J | 25.332 J |
| **Number of functions calls** | 4 | 208 |

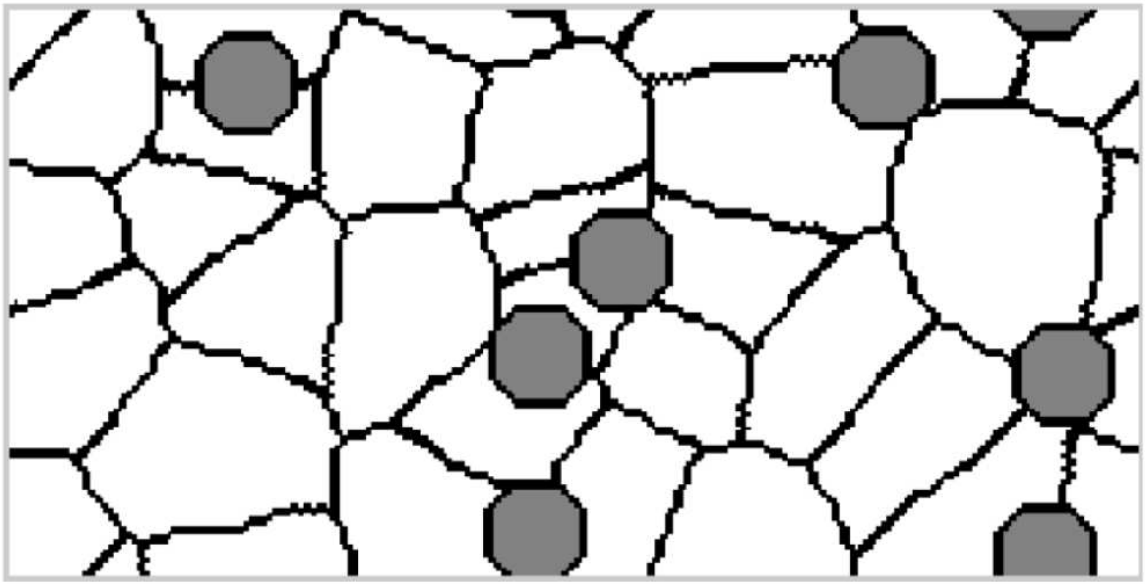

Figure 5.4. Optimal morphology for input temperature 1400°Cand $\alpha = 0.5$

### 5.2.4 Temperature 25°Cand $\alpha = 0.5$

By using $\omega = 1$ we consider only the sample for temperature 25°C. By using $\alpha = 0.5$ we take 50% weightage of the uncertainties in the design. Quadratic surface polynomials at every point of the fracture energy are generated to create a surrogate model. Every sample is tested 20 times to quantify the uncertainty. The standard deviations of fracture energies for both the temperatures were around 3.7.

The optimized result is as shown in the Figure 5.5. The optimum result obtained is $[4, 11]$.Hence the average size of the SiC particles is 800 nanometers.

Table 5.7. Results for Temperature 25°Cand $\alpha = 0.5$

| | **High Fidelity Model** | **Surrogate Model** |
|---|---|---|
| **Fracture Energy** | 19.736 J | 19.582 J |
| **Number of functions calls** | 8 | 389 |

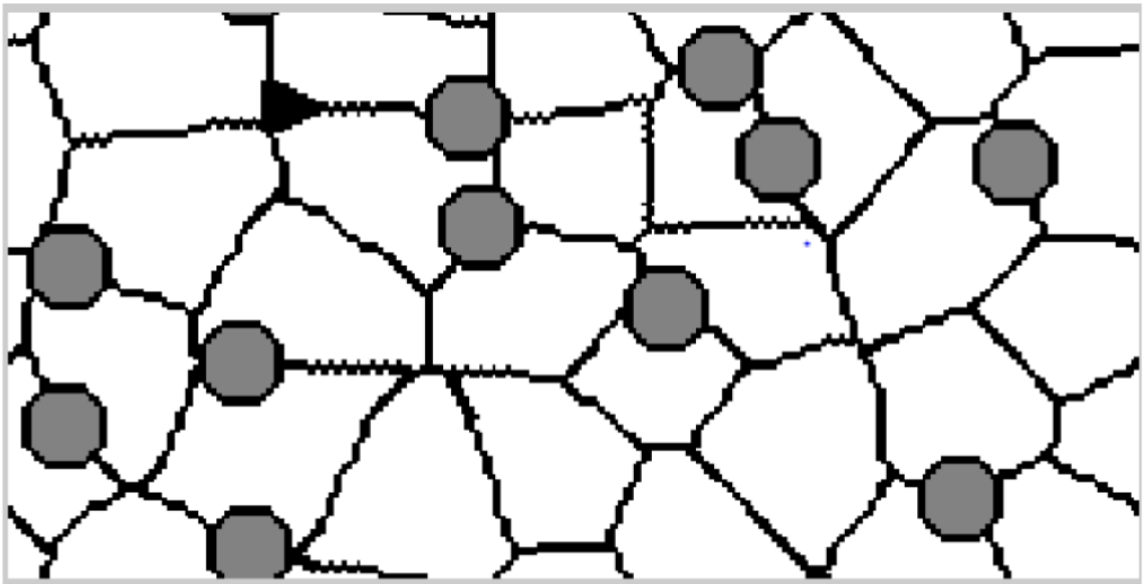

Figure 5.5. Optimal morphology for input temperature 25°Cand $\alpha = 0.5$

## 5.3 Summary

The goal of this research is to find the optimal morphology of the composite at low and high temperatures while incorporating the robust optimization algorithm along with reduction in computational cost.

### 5.3.1 Material Design using Surrogate Optimization Algorithm

A surrogate model is integrated in the material design framework to reduce the number of high fidelity function calls. The above methodology proves in generating

feasible and optimal optimal hybrid material morphologies with targeted material properties. A summary of the optimization framework is as shown in Figure 5.6.

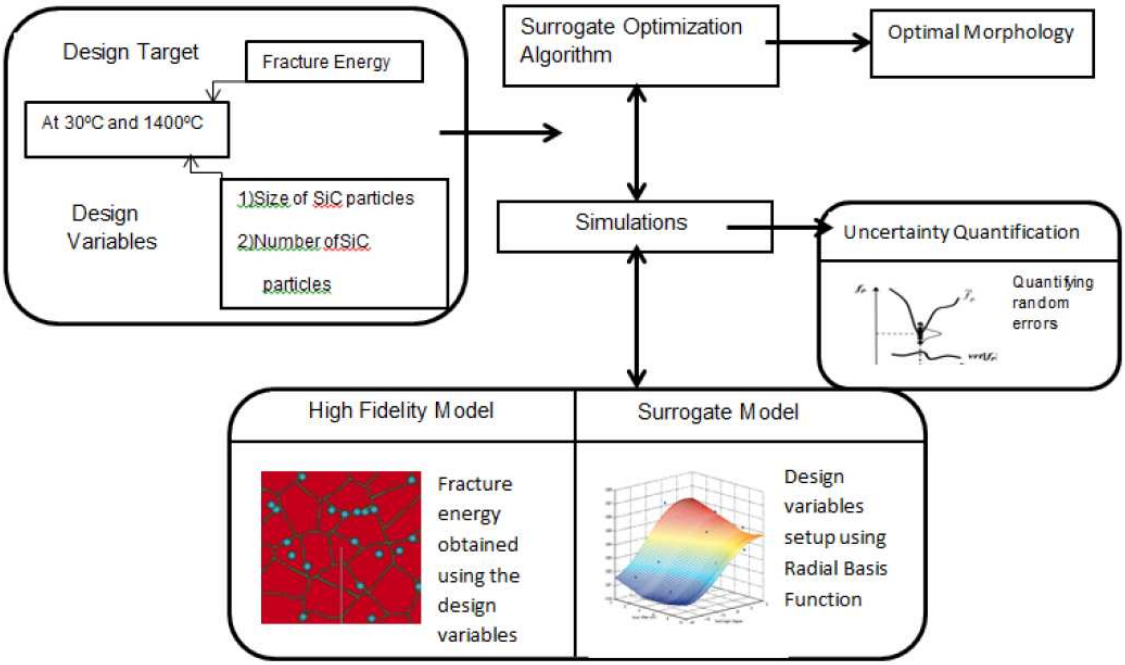


Figure 5.6. Structural integration of the investigation

**Investigation # $\omega = 0.5$ and $\alpha = 1$**

In this investigation the target result was achieved in 227 surrogate model calls and 5 high fidelity function calls. The target numbers of SiC particles found for this input were 10 and its size 3 (600 nanometers).The surrogate model optimization algorithm was therefore effective in maximizing the fracture energy of the composite material. The surrogate model was developed using the radial basis function to minimize the optimization time.

**Investigation # Temperature 1400°Cand** $\alpha = 1$

In this investigation the target result was achieved in 208 surrogate model calls and 4 high fidelity function calls. The target number of SiC particles found for this input were 7 and its size 5 (1000 nanometers).The result proves that increase in the size of the SiC particles is necessary for the crack bridging effect at elevated temperatures due to the weakening of the grain boundaries [19, 22].The amount of SiC particles required are less because these can be effective enough to divert the fracture path [26, 29].

**Investigation # Temperature 25°Cand** $\alpha = 1$

In this investigation the target result was achieved in 389 surrogate model calls and 8 high fidelity function calls. The target numbers of SiC particles found for this input were 11 and its size 4 (800 nanometers).The size of the SiC particles required to increase the fracture energy at room temperature may not be as high as compared to the size at 1400oC because the SiC flexural properties are higher than at room temperature [31–36]. Also the grain boundaries are stronger at room temperature so they only need the SiC nanoparticles to prevent the grain boundary sliding effect [27, 29].

# 6. CONCLUSIONS AND FUTURE WORK

## 6.1 Conclusion

The research introduces a methodology to find the optimal morphology of a composite material at various temperatures. The design optimization framework incorporates surrogate algorithm in the optimization framework. The CA model is introduced for microstructure generation and the random errors in its generation are also quantified making the optimization robust [1]. The design methodology is applied to three different test problems. The results show that the number of silicon carbide particles and its size has varied for 25°Cand 1400°Cbased on the fracture energy of the material. At 25°Cthe preferred material is the one with higher number of silicon carbide particles but with small size and at 1400°Cthe preferred material is exactly the opposite. In all the three cases it calls the high fidelity model less than 9 times which is a significant reduction to optimize this design model. The results obtained not only give a comprehensive overview on the optimal morphology of the composite material but also reduces the optimization time.

Thus this methodology can also be extended for optimizing the morphology of any multiphase composite material.

## 6.2 Future work

### 6.2.1 Apply the algorithm to a 3D high fidelity model

The present algorithm can be applied to a 3D high fidelity for more better solutions. But a compromise has to be made between the design time and the fidelity of the model. Also a scaling function will have to be introduced in the algorithm for making it more accurate.

### 6.2.2 Increasing the number of design variables

The number of design variables in the optimization algorithm can also be increased by including also the size and the number of $Si_3N_4$ particles. Also the adding the size of the grain boundary as a design variable can also prove to effective for maximizing its fracture energy.

### 6.2.3 Incorporate higher physics models in the optimization algorithm

The physics involved in the structure of the $Si_3N_4$-SiC is not completely represented in this work. High temperature plastic behavior, atomic behavior and cohesive fracture are some of physical features that can be incorporated in the high fidelity model [1]. Hence research can be done in conjecture with scientists involved in experimentation of these composite materials.

### 6.2.4 Experimental testing of methodology

Physical experiments are needed to validate the results obtained in this investigation. This will effectively prove the capability of this methodology in material design. For this purpose, collaborative research is needed with experimentalists.

# REFERENCES

# REFERENCES


[1] S. Bose and J. DeMasi-Marcin, "Thermal barrier coating experience in gas turbine engines at pratt & whitney," *Journal of Thermal Spray Technology*, vol. 6, no. 1, pp. 99–104, 1997.

[2] N. Q. Minh, "Ceramic fuel cells," *Journal of the American Ceramic Society*, vol. 76, no. 3, pp. 563–588, 1993.

[3] X. Qu, R. T. Haftka, S. Venkataraman, and T. F. Johnson, "Deterministic and reliability-based optimization of composite laminates for cryogenic environments," *AIAA journal*, vol. 41, no. 10, pp. 2029–2036, 2003.

[4] R. T. Haftka *et al.*, *Elements of structural optimization*. Springer, 1992, vol. 11.

[5] C.-G. Aronsson and J. Backlund, "Tensile fracture of laminates with cracks," *Journal of composite materials*, vol. 20, no. 3, pp. 287–307, 1986.

[6] Y. Liu, M. Steven Greene, W. Chen, D. A. Dikin, and W. K. Liu, "Computational microstructure characterization and reconstruction for stochastic multiscale material design," *Computer-Aided Design*, vol. 45, no. 1, pp. 65–76, 2013.

[7] H. Xu, D. A. Dikin, C. Burkhart, and W. Chen, "Descriptor-based methodology for statistical characterization and 3d reconstruction of microstructural materials," *Computational Materials Science*, vol. 85, pp. 206–216, 2014.

[8] C. C. Seepersad, B. Dempsey, J. K. Allen, F. Mistree, and D. L. McDowell, "Design of multifunctional honeycomb materials," *AIAA journal*, vol. 42, no. 5, pp. 1025–1033, 2004.

[9] S. Omkar, J. Senthilnath, R. Khandelwal, G. Narayana Naik, and S. Gopalakrishnan, "Artificial bee colony (abc) for multi-objective design optimization of composite structures," *Applied Soft Computing*, vol. 11, no. 1, pp. 489–499, 2011.

[10] H. Ghiasi, K. Fayazbakhsh, D. Pasini, and L. Lessard, "Optimum stacking sequence design of composite materials part ii: Variable stiffness design," *Composite Structures*, vol. 93, no. 1, pp. 1–13, 2010.

[11] X. Martinez, F. Rastellini, S. Oller, F. Flores, and E. Oñate, "Computationally optimized formulation for the simulation of composite materials and delamination failures," *Composites Part B: Engineering*, vol. 42, no. 2, pp. 134–144, 2011.

[12] A. A. Pelegri and A. Tekkam, "Optimization of laminates fracture toughness using design of experiments and response surface," *Journal of composite materials*, vol. 37, no. 7, pp. 579–596, 2003.

[13] P. P. Camanho, C. G. Dávila, and D. R. Ambur, *Numerical simulation of delamination growth in composite materials*. Citeseer, 2001.

[14] P. P. Camanho, C. Davila, and M. De Moura, "Numerical simulation of mixed-mode progressive delamination in composite materials," *Journal of composite materials*, vol. 37, no. 16, pp. 1415–1438, 2003.

[15] H. Park, H.-E. Kim, and K. Niihara, "Microstructure and high-temperature strength of si¡ sub¿ 3¡/sub¿ n¡ sub¿ 4¡/sub¿-sic nanocomposite," *Journal of the European ceramic society*, vol. 18, no. 7, pp. 907–914, 1998.

[16] J. J. Swab, A. A. Wereszczak, K. T. Strong, D. Danna, J. C. LaSalvia, M. E. Ragan, and P. J. Ritt, "Knoop hardness–apparent yield stress relationship in ceramics," *International Journal of Applied Ceramic Technology*, vol. 9, no. 3, pp. 650–655, 2012.

[17] Y. S. Ong, P. B. Nair, and A. J. Keane, "Evolutionary optimization of computationally expensive problems via surrogate modeling," *AIAA journal*, vol. 41, no. 4, pp. 687–696, 2003.

[18] N. V. Queipo, R. T. Haftka, W. Shyy, T. Goel, R. Vaidyanathan, and P. Kevin Tucker, "Surrogate-based analysis and optimization," *Progress in aerospace sciences*, vol. 41, no. 1, pp. 1–28, 2005.

[19] D. Weaire, J. Kermode, and J. Wejchert, "On the distribution of cell areas in a voronoi network," *Philosophical Magazine B*, vol. 53, no. 5, pp. L101–L105, 1986.

[20] D.-T. Lee and A. K. Lin, "Generalized delaunay triangulation for planar graphs," *Discrete & Computational Geometry*, vol. 1, no. 1, pp. 201–217, 1986.

[21] K. W. Mahin, K. Hanson, and J. Morris Jr, "Comparative analysis of the cellular and johnson-mehl microstructures through computer simulation," *Acta Metallurgica*, vol. 28, no. 4, pp. 443–453, 1980.

[22] S. Brown, "Simulation of diffusional composite growth using the cellular automaton finite difference (cafd) method," *Journal of materials science*, vol. 33, no. 19, pp. 4769–4773, 1998.

[23] H. H. Xu, L. M. Braun, C. P. Ostertag, R. F. Krause, and I. K. Lloyd, "Failure modes of sic-fiber/si3n4-matrix composites at elevated temperatures," *Journal of the American Ceramic Society*, vol. 78, no. 2, pp. 388–394, 1995.

[24] R. John, L. P. Zawada, and J. L. Kroupa, "Stresses due to temperature gradients in ceramic-matrix-composite aerospace components," *Journal of the American Ceramic Society*, vol. 82, no. 1, pp. 161–168, 1999.

[25] C. R. Jones, C. H. Henager Jr, and R. H. Jones, "Crack bridging by sic fibers during slow crack growth and the resultant fracture toughness of sicsicf composites," *Scripta metallurgica et materialia*, vol. 33, no. 12, pp. 2067–2072, 1995.

[26] G. Boyd and D. Kreiner, "Agt101/attap ceramic technology development," *Journal of Engineering for Gas Turbines and Power*, vol. 111, no. 1, pp. 158–167, 1989.

[27] H. H. Xu, C. P. Ostertag, E. R. Fuller, L. M. Braun, and I. K. Lloyd, "Fracture resistance of sic-fiber-reinforced si3n4 composites at ambient and elevated temperatures," *Journal of the American Ceramic Society*, vol. 78, no. 3, pp. 698–704, 1995.

[28] Y. Gogotsi and V. Domnich, *High pressure surface science and engineering*. CRC Press, 2010.

[29] A. Lakki and R. Schaller, "High temperature microplasticity of fine-grained ceramics," *Le Journal de Physique IV*, vol. 6, no. C8, pp. C8–331, 1996.

[30] V. Domnich, Y. Gogotsi, and S. Dub, "Effect of phase transformations on the shape of the unloading curve in the nanoindentation of silicon," *Applied Physics Letters*, vol. 76, no. 16, pp. 2214–2216, 2000.

[31] J. Limido, C. Espinosa, M. Salaün, and J.-L. Lacome, "Sph method applied to high speed cutting modelling," *International journal of mechanical sciences*, vol. 49, no. 7, pp. 898–908, 2007.

[32] M. Christ, G. Thurn, M. Weinmann, J. Bill, and F. Aldinger, "High-temperature mechanical properties of si-b-c-n-precursor-derived amorphous ceramics and the applicability of deformation models developed for metallic glasses," *Journal of the American Ceramic Society*, vol. 83, no. 12, pp. 3025–3032, 2000.

[33] C.-M. Wang, X. Pan, M. Rühle, F. Riley, and M. Mitomo, "Silicon nitride crystal structure and observations of lattice defects," *Journal of materials science*, vol. 31, no. 20, pp. 5281–5298, 1996.

[34] A. H. Jones, R. Dobedoe, and M. Lewis, "Mechanical properties and tribology of si¡ sub¿ 3¡/sub¿ n¡ sub¿ 4¡/sub¿–tib¡ sub¿ 2¡/sub¿ ceramic composites produced by hot pressing and hot isostatic pressing," *Journal of the European Ceramic Society*, vol. 21, no. 7, pp. 969–980, 2001.

[35] R. Kottada and A. Chokshi, "Grain boundary sliding during diffusion and dislocation creep in a mg-0.7 pct al alloy," *Metallurgical and Materials Transactions A*, vol. 38, no. 8, pp. 1743–1749, 2007.

[36] J. Gubicza, P. Arató, and F. Wéber, "Oxidation-induced changes in mechanical properties of silicon nitride ceramics," *Advances in science and technology*, pp. A743–A750, 1999.

[37] U. Ramamurty, A. Kim, S. Suresh, and J. Petrovic, "Micromechanisms of creep–fatigue crack growth in a silicide-matrix composite with sic particles," *Journal of the American Ceramic Society*, vol. 76, no. 8, pp. 1953–1964, 1993.

[38] S. U. Din and P. S. NICHOLSON, "Creep deformation of reaction-sintered silicon nitrides," *Journal of the American Ceramic Society*, vol. 58, no. 11-12, pp. 500–502, 1975.

[39] T. Kusunose, T. Sekino, Y. H. Choa, and K. Niihara, "Fabrication and microstructure of silicon nitride/boron nitride nanocomposites," *Journal of the American Ceramic Society*, vol. 85, no. 11, pp. 2678–2688, 2002.

[40] P. Klimczyk, "Mechanical properties of si3n4-sic composites sintered by hpht method," *Advances in Science and Technology*, vol. 63, pp. 396–401, 2011.

[41] K. Niihara, "New design concept of structural ceramicsceramic nanocomposites," *Nippon seramikkusu kyokai gakujutsu ronbunshi*, vol. 99, no. 10, pp. 974–982, 1991.

[42] S. Choi and B. V. Sankar, "A micromechanical method to predict the fracture toughness of cellular materials," *International journal of solids and structures*, vol. 42, no. 5, pp. 1797–1817, 2005.

[43] J. Gilman, "Relationship between impact yield stress and indentation hardness," *Journal of Applied Physics*, vol. 46, no. 4, pp. 1435–1436, 1975.

[44] G. Blugan, M. Hadad, J. Janczak-Rusch, J. Kuebler, and T. Graule, "Fractography, mechanical properties, and microstructure of commercial silicon nitride–titanium nitride composites," *Journal of the American Ceramic Society*, vol. 88, no. 4, pp. 926–933, 2005.

[45] S. R. Choi and D. L. Krause, "Assessments of mechanical and life limiting properties of two candidate silicon nitrides for stirling convertor heater head applications," 2006.

[46] G. L. Harris, *Properties of silicon carbide*. Iet, 1995, no. 13.

[47] R. K. Kalia, A. Nakano, A. Omeltchenko, K. Tsuruta, and P. Vashishta, "Role of ultrafine microstructures in dynamic fracture in nanophase silicon nitride," *Physical review letters*, vol. 78, no. 11, p. 2144, 1997.

[48] M. KAŠIAROVÁ, J. DUSZA, M. HNATKO, and P. ŠAJGALÍK, "Microstructure and mechanical properties of si3n4-sic nanocomposites."

[49] K. Niihara, A. Nakahira, and T. Sekino, "New nanocomposite structural ceramics," in *MRS Proceedings*, vol. 286. Cambridge Univ Press, 1992, p. 405.

[50] J. Qian, C. Pantea, J. Zhang, L. Daemen, Y. Zhao, M. Tang, T. Uchida, and Y. Wang, "Yield strength of $\alpha$-silicon nitride at high pressure and high temperature," *Journal of the American Ceramic Society*, vol. 88, no. 4, pp. 903–906, 2005.

[51] G. Mejía-Rodríguez, J. E. Renaud, and V. Tomar, "A variable fidelity model management framework for designing multiphase materials," *Journal of Mechanical Design*, vol. 130, no. 9, p. 091702, 2008.

[52] W. H. Gerstle and M. Xie, "Fem modeling of fictitious crack propagation in concrete," *Journal of Engineering Mechanics*, vol. 118, no. 2, pp. 416–434, 1992.

[53] T. L. Anderson, *Fracture mechanics: fundamentals and applications*. CRC press, 2005.

[54] V. Tomar and M. Zhou, "Deterministic and stochastic analyses of dynamic fracture in two-phase ceramic microstructures with random material properties," *Eng. Fract. Mech*, vol. 72, no. 12, pp. 1920–1941, 2005.

[55] J. Zhai, V. Tomar, and M. Zhou, "Micromechanical simulation of dynamic fracture using the cohesive finite element method," *Journal of engineering materials and technology*, vol. 126, no. 2, pp. 179–191, 2004.

[56] L.-D. LSTC, "keyword users manual," *Version*, vol. 960, pp. 1–2, 2003.

[57] T. Ohji, Y.-K. Jeong, Y.-H. Choa, and K. Niihara, "Strengthening and toughening mechanisms of ceramic nanocomposites," *Journal of the American Ceramic Society*, vol. 81, no. 6, pp. 1453–1460, 1998.

[58] Z. Qian, C. C. Seepersad, V. R. Joseph, J. K. Allen, and C. J. Wu, "Building surrogate models based on detailed and approximate simulations," *Journal of Mechanical Design*, vol. 128, no. 4, pp. 668–677, 2006.

[59] L. E. Weiss, C. H. Amon, S. Finger, E. D. Miller, D. Romero, I. Verdinelli, L. Walker, and P. G. Campbell, "Bayesian computer-aided experimental design of heterogeneous scaffolds for tissue engineering," *Computer-Aided Design*, vol. 37, no. 11, pp. 1127–1139, 2005.

[60] V. M. Pérez, J. E. Renaud, and L. T. Watson, "An interior-point sequential approximate optimization methodology," *Structural and Multidisciplinary Optimization*, vol. 27, no. 5, pp. 360–370, 2004.

[61] D. S. Broomhead and D. Lowe, "Radial basis functions, multi-variable functional interpolation and adaptive networks," DTIC Document, Tech. Rep., 1988.

[62] J. Park and I. W. Sandberg, "Universal approximation using radial-basis-function networks," *Neural computation*, vol. 3, no. 2, pp. 246–257, 1991.

[63] Y.-S. Ong, K. Y. Lum, and P. B. Nair, "Hybrid evolutionary algorithm with hermite radial basis function interpolants for computationally expensive adjoint solvers," *Computational Optimization and Applications*, vol. 39, no. 1, pp. 97–119, 2008.

[64] T. W. Simpson, T. M. Mauery, J. J. Korte, and F. Mistree, "Kriging models for global approximation in simulation-based multidisciplinary design optimization," *AIAA journal*, vol. 39, no. 12, pp. 2233–2241, 2001.

[65] S. Jeong, M. Murayama, and K. Yamamoto, "Efficient optimization design method using kriging model," *Journal of Aircraft*, vol. 42, no. 2, pp. 413–420, 2005.

[66] J. W. Bandler and K. Madsen, "Editorialsurrogate modelling and space mapping for engineering optimization," *Optimization and Engineering*, vol. 2, no. 4, pp. 367–368, 2001.

[67] A. A. Giunta, S. F. Wojtkiewicz, M. S. Eldred *et al.*, "Overview of modern design of experiments methods for computational simulations," in *Proceedings of the 41st AIAA Aerospace Sciences Meeting and Exhibit, AIAA-2003-0649*, 2003.

[68] M. D. McKay, "Latin hypercube sampling as a tool in uncertainty analysis of computer models," in *Proceedings of the 24th conference on Winter simulation*. ACM, 1992, pp. 557–564.

[69] M. E. Johnson, L. M. Moore, and D. Ylvisaker, "Minimax and maximin distance designs," *Journal of statistical planning and inference*, vol. 26, no. 2, pp. 131–148, 1990.

[70] M. D. Morris and T. J. Mitchell, "Exploratory designs for computational experiments," *Journal of statistical planning and inference*, vol. 43, no. 3, pp. 381–402, 1995.

[71] V. R. Joseph and Y. Hung, "Orthogonal-maximin latin hypercube designs," *Statistica Sinica*, vol. 18, no. 1, p. 171, 2008.

[72] M. D. Buhmann, "Radial basis functions," *Acta Numerica 2000*, vol. 9, pp. 1–38, 2000.

[73] M. J. Powell, "A fast algorithm for nonlinearly constrained optimization calculations," in *Numerical analysis*. Springer, 1978, pp. 144–157.

[74] ——, "The convergence of variable metric methods for non-linearly constrained optimization calculations," *Nonlinear programming*, vol. 3, 1978.

[75] P. E. Gill, W. Murray, and M. H. Wright, "Practical optimization," 1981.

[76] G. Taguchi and D. Clausing, "Robust quality," *Harvard Business Review*, vol. 68, no. 1, pp. 65–75, 1990.

[77] W. Y. Fowlkes and C. M. Creveling, *Engineering methods for robust product design*. Addison-Wesley, 1995.

[78] X. Du and W. Chen, "Sequential optimization and reliability assessment method for efficient probabilistic design," *Journal of Mechanical Design*, vol. 126, no. 2, pp. 225–233, 2004.

[79] X. Gu and J. E. Renaud, "Implicit uncertainty propagation for robust collaborative optimization," in *Proceedings of DETC01, ASME 2001 Design Engineering Technical Conferences and Computers and Information in Engineering Conference, CD-ROM Proceedings*. Citeseer, 2001.